Fixed-time Autonomous Shipboard Landing Control of a Helicopter with External Disturbances

Yanting Huang[a,b], Ming Zhu[b], Zewei Zheng[a,*], Mir Feroskhan[c]

[a] *The Seventh Research Division, School of Automation Science and Electrical Engineering, Beihang University, Beijing 100191, P.R. China*

[b] *School of Aeronautic Science and Engineering, Beihang University, Beijing 100191, P.R. China*

[c] *School of Mechanical and Aerospace Engineering, Nanyang Technological University, Singapore, 639798*

Abstract

This paper presents a new fixed-time control algorithm to enable autonomous landing of a helicopter onto the ship's deck in the presence of parametric uncertainties and external disturbances. A nonsingular terminal sliding control is implemented as an integral part of the fixed-time control scheme, that guarantees the convergence of system errors to zero in a fixed settling time, however, without the consideration of disturbances. Subsequently, a fixed-time disturbance observer is incorporated into the control structure to efficiently estimate the lumped disturbances including modeling inaccuracies and external perturbations, while reducing the undesired chattering in the control inputs effectively as well. By establishing a relative motion model between the helicopter and the ship, the shipboard landing problem is converted from a general trajectory tracking problem to a more favorable stabilization problem. Based on the fixed-time control scheme in the relative motion model, a relative position controller (RPC) and a relative attitude-altitude controller (RAC) are formulated to guide the helicopter in a dual-phase landing sequence. The RPC will first be implemented to direct the helicopter from its initial position to a hover position above the ship. The next phase involves the application of RAC to guide the helicopter to descend steadily on the ship. Numerical comparative simulations are also carried out to validate the remarkable performance of the proposed control approach.

Keywords: Helicopter, Shipboard Landing, Fixed-time Control, Terminal Sliding Mode, Fixed-time Observer

1. Introduction

A considerable amount of research has been performed on the design, development and operation of helicopters for decades. The helicopter has been widely applied in various fields such as reconnaissance, surveillance and agriculture, as they are capable of vertically taking off and landing (VTOL), hovering and low-speed flight, unlike the fixed-wing aircraft platforms [1]. Particularly, the VTOL functionality allows helicopters to be readily utilized for maritime operations [2]. However, due to the complex motion characteristics of both the helicopter and the ship, which can be further aggravated by the presence of strong wind blowing, unpredictable sea currents and a relatively narrow deck space, the shipboard landing maneuver becomes a precarious and challenging procedure [3].

The autonomous landing methods on a fixed platform have been widely studied [4, 5]. Likewise, numerous approaches for the landing on moving targets have also been studied. For instance, an algorithm that consists of a guidance law and a time-delay controller was developed in [2] for landing a helicopter on a shipboard in the presence of model uncertainties and crosswind. Alternatively, an autonomous control algorithm for landing a quadrotor on a moving mobile platform, which is based on the backstepping and dynamic surface control, was proposed in [6]. An optimization approach was utilized in an automatic carrier landing system [7] as well, in which a novel method based on a simplified brain storm optimization algorithm was presented to optimize the control parameters. In addition, vision-guided approaches are vastly applied to solve the autonomous landing problem [8, 9, 10].

However, a majority of the landing platforms covered in aforementioned literature comprise of either simple moving platforms [3, 11], two degree of freedom (DOF) platforms [2, 6, 9] or three DOF platforms [12, 13], which in reality are not representative of the 6-DOF motion characteristics of the ship. As there is hardly any investigation that is based on the use of a 6-DOF moving platform [14], this drives the motivation to extend the study of autonomous shipboard landing on a 6-DOF moving platform that serves as a more accurate characterization of the ship's dynamics. Moveover, the landing techniques described above have researched mainly on the control design for the aircraft to track the motion trajectory of the landing target. Inspired by the application of a relative motion modeling method for a spacecraft rendezvous sys-

*Corresponding author

Email address: zeweizheng@buaa.edu.cn (Zewei Zheng)

tem in [15], a similar relative motion dynamic model is adopted in this paper to capture the relative motion dynamics between the helicopter and ship.

With the goal of attaining a safe and reliable helicopter landing, a high degree of system's robustness to external disturbances becomes a crucial requirement for the landing controller. Therefore, the controller design should be able to effectively nullify the effects of the external disturbances during sea operations. Capability to complete the autonomous landing as fast as possible should also be one of the control goals as it indicates a good landing performance. Indirectly, a prompt landing also reduces the exposure of the external disturbances and its effects to some extent. The option of implementing the finite-time control scheme [16]-[18] that offers a short and finite convergence time to the desired target is plausible. However, its limitation includes that the settling time of the controller would depend on the initial values of the system. An extension of the finite-time convergence concept is fixed-time control method [19, 20], which is able to estimate a fixed maximum settling time regardless of the initial conditions.

A valid technique to achieve a fixed-time convergence property is the terminal sliding mode control (TSMC) [21, 22], which provides a shorter settling time than the traditional sliding mode control [23, 24] due to the application of the non-linear switching manifolds. The terminal sliding mode tracking control with finite-time disturbance observer was proposed for the signal-input and signal-output nonlinear system in [25]. The work in [26] utilized a fixed-time stable first-order system for the network consensus problem. Jiang [16] designed a fixed-time fault-tolerant controller that compensates for the external disturbances and thrust faults. Nevertheless, a singularity problem may occur in aforementioned works if the initial conditions are selected improperly, which would unfortunately result in infinite control inputs. To overcome the singularity problem, several control strategies have been investigated. In [27], a modified TSMC was investigated to totally avoid the possibility of the singularity occurrence. Zuo [19] independently proposed a newly defined non-singular terminal sliding surface under matched system uncertainties and perturbations. Although the control methods presented in [19] and [27] are shown to reduce the chattering effects in the control inputs, they are still not able to eliminate chattering phenomenon entirely. The resulting control inputs that are discontinuous may lead to the degradation of the actuator's performance.

It has been shown in literature that the disturbances encountered by a system can be estimated using disturbance observers (DO) such as nonlinear DO [28, 29], finite-time DO [30]-[32] and fixed-time DO [33, 34]. Generally, continuous finite-time or fixed-time DO are designed via utilizing higher-order sliding mode [30, 31, 33] or homogeneous system theory [32, 34]. Based on the finite-time DO, [31] proposed a novel nonlinear sliding mode surface that involves mismatched disturbance attenuation. The observers designed in [34] allows the estimation of actuator faults and model uncertainties with the corresponding estimation errors undergoing fixed-time convergence to zero. As such, the fixed-time DO that guarantees a specified convergence time regardless of initial conditions is proposed for the autonomous shipboard landing of a helicopter using the relative motion model under parametric uncertainties and external disturbances.

To account for the under-actuated problem of the relative motion model, the entire autonomous landing operation involves two phases: the approach phase and the descent phase (see in Fig. 1) [35]. In the first stage, the helicopter is tasked to advance towards the ship and achieve hover above the ship by using a relative position control (RPC). In the second stage, the helicopter descends vertically to the ship by using a relative attitude-altitude control (RAC). The main contributions of this paper are summarized as follows: (i) A new fixed-time autonomous ship landing control method is designed using a combination of the nonsingular terminal sliding mode technique and the fixed-time DO. The upper boundary of the total settling time can subsequently be calculated. (ii) The fixed-time DO are incorporated to estimate the lump disturbances in both RPC and RAC. In this case, the control signals of the proposed algorithm are ensured to be smooth which consecutively offers better chattering attenuation than the existing TSMC. (iii) The landing position errors are addressed by Monte-Carlo simulations to verify the robustness and reliability of the proposed controllers when subjected to random perturbations.

The layout of the paper is arranged as follows. Some preliminaries are presented in Sect. 2. The 6-DOF relative model and objective are described in Sect. 3. Sect. 4 is devoted to detailing the design of RPC and RAC. In Sect. 5, numerical simulations are performed to verify the proposed approach, followed by the conclusion in Sect. 6.

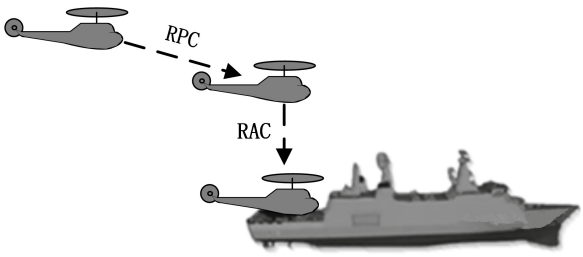

Figure 1: The process of automatic landing

2. Preliminaries

Throughout this paper, the following notations are adopted. $|\cdot|$ denotes the absolute value of a scalar or the absolute value of each components for a vector, $\|\cdot\|$ refers to the Euclidean norm of a vector or the Frobenius norm of a matrix. For a vector $\boldsymbol{x} = [x_1, x_2, \cdots, x_n]^T \in \mathbb{R}^n$

and a scalar $k \in \mathbb{R}$, $\langle \boldsymbol{x} \rangle = \text{diag}\{x_1, x_2, \cdots, x_n\}$ and $\boldsymbol{x}^{\lceil k \rfloor} = [x_1^k, x_2^k, \cdots, x_n^k]^T$. $\lambda_{\min}(\boldsymbol{A})$ specifies the minimum eigenvalue of a square matrix $\boldsymbol{A}$.

Consider the system

$$\dot{\boldsymbol{x}}(t) = \boldsymbol{f}(\boldsymbol{x}(t)), \boldsymbol{x}(0) = \boldsymbol{x}_0, \boldsymbol{f}(\boldsymbol{0}) = 0, \boldsymbol{x} \in \mathbb{R}^n \quad (1)$$

where $\boldsymbol{f} : D_0 \to \mathbb{R}^n$ is continuous on an open neighborhood D_0 of the origin.

Definition 1. *[36] The equilibrium point $\boldsymbol{x} = 0$ of (1) is said to be fixed-time stable if it is globally finite-time stable and the settling time function $T(\boldsymbol{x}_0)$ is bounded, that is, there exists a $T_{max} > 0$ such that $T(\boldsymbol{x}_0) < T_{max}$ for any $\boldsymbol{x}_0 \in \mathbb{R}^n$.*

Lemma 1. *[37] Consider a system*

$$\dot{\boldsymbol{y}} = -\alpha \boldsymbol{y}^{\lceil \frac{m}{n} \rfloor} - \beta \boldsymbol{y}^{\lceil \frac{p}{q} \rfloor}, \boldsymbol{y}(0) = \boldsymbol{y}_0, \boldsymbol{y} \in \mathbb{R}^n \quad (2)$$

where $\alpha > 0$, $\beta > 0$ and m, n, p, q are positive odd integers satisfying $m > n$ and $p < q$. Then the equilibrium of (2) is fixed-time stable and the settling time T is bounded by $T < \frac{1}{\alpha}\frac{n}{m-n} + \frac{1}{\beta}\frac{q}{q-p}$.

Lemma 2. *[38] For any $x_i \in \mathbb{R}$, if $k \in \mathbb{R}^+$, then $(|x_1| + |x_2| + \cdots + |x_n|)^k \leq max(n^{k-1}, 1)(|x_1|^k + |x_2|^k + \cdots + |x_n|^k)$.*

3. Problem Formulation

3.1. Reference frames

The related frames are illustrated in Fig.2. As shown in Fig.2, the inertial frame and body-fixed frames of the helicopter and the ship are defined respectively. The inertial frame $\mathcal{F}_e = \{O_e, \boldsymbol{x_e}, \boldsymbol{y_e}, \boldsymbol{z_e}\}$ is fixed on the earth. The frames $\mathcal{F}_q = \{O_q, \boldsymbol{x_q}, \boldsymbol{y_q}, \boldsymbol{z_q}\}$ and $\mathcal{F}_c = \{O_c, \boldsymbol{x_c}, \boldsymbol{y_c}, \boldsymbol{z_c}\}$ represent the body frames of the helicopter and the ship, respectively. O_q and O_c are the geometric center points of the helicopter and the ship, respectively.

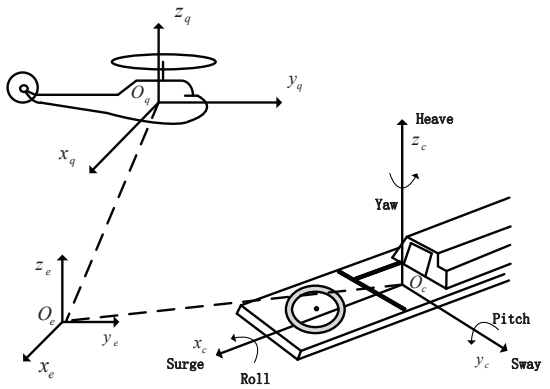

Figure 2: Reference frames

3.2. Models of the Helicopter and the Ship

Using 'Newton-Euler' formulae, the helicopter model [39] can be derived as

$$\begin{cases} \dot{\boldsymbol{\xi}}_1 = \boldsymbol{V}_1 \\ m\dot{\boldsymbol{V}}_1 = -mg\boldsymbol{e}_3 + \boldsymbol{R}_{t_1}\boldsymbol{f} + \boldsymbol{d}_f \\ \dot{\boldsymbol{\eta}}_1 = \boldsymbol{R}_{r_1}\boldsymbol{\Omega}_1 \\ \boldsymbol{I}\dot{\boldsymbol{\Omega}}_1 = -\boldsymbol{\Omega}_1 \times \boldsymbol{I}\boldsymbol{\Omega}_1 + \boldsymbol{\tau} + \boldsymbol{d}_\tau \end{cases} \quad (3)$$

where $\boldsymbol{\xi}_1 = [x_1, y_1, z_1]^T$, $\boldsymbol{\eta}_1 = [\phi_1, \theta_1, \psi_1]^T$ and $\boldsymbol{V}_1 = [u_1, v_1, w_1]^T$ represent the position vector, the attitude vector and the velocity vector of helicopter in the frame $\mathcal{F}_e$, respectively. $\boldsymbol{\Omega}_1 = [p_1, q_1, r_1]^T$ is the angular velocity vector in the frame $\mathcal{F}_q$. In addition, $\boldsymbol{e}_3 = [0, 0, 1]^T$ and g is the gravity constant. m and $\boldsymbol{I} = \text{diag}(I_x, I_y, I_z)$ denote the total mass and inertial moment matrix, respectively. $\boldsymbol{d}_f$ and $\boldsymbol{d}_\tau$ describe the aerodynamic disturbances such as turbulence and gusts modeled in the simulations section. The rotation matrix $\boldsymbol{R}_{t_1}$ and transformation matrix $\boldsymbol{R}_{r_1}$ are given by

$$\boldsymbol{R}_{t_1} = \begin{bmatrix} \text{c}_{\theta_1}\text{c}_{\psi_1} & \text{s}_{\theta_1}\text{c}_{\psi_1}\text{s}_{\phi_1} - \text{s}_{\psi_1}\text{c}_{\phi_1} & \text{s}_{\theta_1}\text{c}_{\psi_1}\text{c}_{\phi_1} + \text{s}_{\psi_1}\text{s}_{\phi_1} \\ \text{c}_{\theta_1}\text{s}_{\psi_1} & \text{s}_{\theta_1}\text{s}_{\psi_1}\text{s}_{\phi_1} + \text{c}_{\psi_1}\text{c}_{\phi_1} & \text{s}_{\theta_1}\text{s}_{\psi_1}\text{c}_{\phi_1} - \text{c}_{\psi_1}\text{s}_{\phi_1} \\ -\text{s}_{\theta_1} & \text{c}_{\theta_1}\text{s}_{\phi_1} & \text{c}_{\theta_1}\text{c}_{\phi_1} \end{bmatrix}$$

$$\boldsymbol{R}_{r_1} = \frac{1}{\text{c}_{\theta_1}} \begin{bmatrix} \text{c}_{\theta_1} & \text{s}_{\phi_1}\text{s}_{\theta_1} & \text{c}_{\phi_1}\text{s}_{\theta_1} \\ 0 & \text{c}_{\phi_1}\text{c}_{\theta_1} & -\text{s}_{\phi_1}\text{c}_{\theta_1} \\ 0 & \text{s}_{\phi_1} & \text{c}_{\phi_1} \end{bmatrix}$$

where $\text{s}_{(\cdot)} \triangleq \sin(\cdot)$, $\text{c}_{(\cdot)} \triangleq \cos(\cdot)$. In addition, we can define $\dot{\boldsymbol{R}}_{t_1} = \boldsymbol{R}_{t_1}\boldsymbol{S}(\boldsymbol{\Omega}_1)$, where $\boldsymbol{S}(\boldsymbol{\Omega}_1)$ is the skew-symmetric matrix defined as

$$\boldsymbol{S}(\boldsymbol{\Omega}_1) = \begin{bmatrix} 0 & -r_1 & q_1 \\ r_1 & 0 & -p_1 \\ -q_1 & p_1 & 0 \end{bmatrix}$$

The acting forces $\boldsymbol{f}$ and torques $\boldsymbol{\tau}$ on the helicopter are mainly generated by the main and tail rotors, which can be computed using the following expressions

$$\boldsymbol{f} = \begin{bmatrix} T_m \text{s}_{a_s} \\ -T_m \text{s}_{b_s} + T_t \\ T_m \text{c}_{a_s}\text{c}_{b_s} \end{bmatrix}$$

$$\boldsymbol{\tau} = \begin{bmatrix} T_m h_m \text{s}_{b_s} + L_b b_s + T_t h_t + \tau_m \text{s}_{a_s} \\ T_m l_m + T_m h_m \text{s}_{a_s} + M_a a_s + \tau_t - \tau_m \text{s}_{b_s} \\ -T_m l_m \text{s}_{b_s} - T_t l_t + \tau_m \text{c}_{a_s}\text{c}_{b_s} \end{bmatrix}$$

where T_i and τ_i $(i = m, t)$ refer to the thrust and antitorque generated by the main or tail rotor, a_s and b_s are the longitudinal and lateral flapping angles, h_i and l_i $(i = m, t)$ indicate the horizontal and vertical positions of the center of the main or tail rotor of the helicopter. L_b and M_a are the longitudinal and lateral stiffness coefficients of the main rotor. $\tau_i (i = m, t)$ is determined by

$$\tau_i = C_i |T_i|^{1.5} + D_i$$

where C_i and D_i are the aerodynamic constants.

Due to the strong coupling property of helicopter, it is necessary to simplify the force $\boldsymbol{f}$ and torque $\boldsymbol{\tau}$ formulations to streamline the control approach design. Since the flapping angles are generally small during flight, the small angle approximation can hence be used, that is, $\cos(\cdot) \approx 1$ and $\sin(\cdot) \approx 0$. Furthermore, $T_m a_s$, $T_m b_s$, T_t and τ_t have negligible effect on force $\boldsymbol{f}$ and torque $\boldsymbol{\tau}$. Therefore, the helicopter model can be simplified as [39]

$$\begin{cases} \dot{\boldsymbol{\xi}}_1 = \boldsymbol{V}_1 \\ \dot{\boldsymbol{V}}_1 = -g\boldsymbol{e}_3 + \dfrac{T_m}{m}\boldsymbol{R}_{t_1}\boldsymbol{e}_3 + \Delta\boldsymbol{f} \\ \dot{\boldsymbol{\eta}}_1 = \boldsymbol{R}_{r_1}\boldsymbol{\Omega}_1 \\ \boldsymbol{I}\dot{\boldsymbol{\Omega}}_1 = -\boldsymbol{\Omega}_1 \times \boldsymbol{I}\boldsymbol{\Omega}_1 + \boldsymbol{\tau}_\gamma + \Delta\boldsymbol{\tau} \end{cases} \tag{4}$$

where T_m and $\boldsymbol{\tau}_\gamma = \boldsymbol{A}_\tau \boldsymbol{M} + \boldsymbol{\tau}_B$ are the control inputs to be designed in the later section. Also,

$$\boldsymbol{A}_\tau = \begin{bmatrix} h_t & \tau_m & T_m h_m + L_b \\ 0 & T_m h_m + M_a & -\tau_m \\ -l_t & 0 & -T_m l_m \end{bmatrix},$$

$$\boldsymbol{M} = \begin{bmatrix} T_t \\ a_s \\ b_s \end{bmatrix}, \qquad \boldsymbol{\tau}_B = \begin{bmatrix} 0 \\ T_m l_m \\ \tau_m \end{bmatrix}.$$

$\Delta\boldsymbol{f} = \boldsymbol{R}_{t_1}\boldsymbol{f}_\Delta + \boldsymbol{d}_f$ and $\Delta\boldsymbol{\tau} = \boldsymbol{\tau}_\Delta + \boldsymbol{d}_\tau$ are treated as the combination of unmodeled dynamics, parametric uncertainties and external disturbances, which will be estimated and compensated with the fixed-time disturbance observer. The external disturbances include the aerodynamic disturbances such as turbulence and gusts modeled in the simulations section. Therefore,

$$\boldsymbol{f}_\Delta = \begin{bmatrix} T_m \mathrm{s}_{a_s} \\ -T_m \mathrm{s}_{b_s} + T_t \\ T_m(\mathrm{c}_{a_s}\mathrm{c}_{b_s} - 1) \end{bmatrix},$$

$$\boldsymbol{\tau}_\Delta = \begin{bmatrix} \tau_m(\mathrm{s}_{a_s} - a_s) + T_m h_m(\mathrm{s}_{b_s} - b_s) \\ \tau_t - \tau_m(\mathrm{s}_{b_s} - b_s) + T_m h_m(\mathrm{s}_{a_s} - a_s) \\ \tau_m(\mathrm{c}_{a_s}\mathrm{c}_{b_s} - 1) - T_m l_m(\mathrm{s}_{b_s} - b_s) \end{bmatrix}.$$

Remark 1. *The error components $\boldsymbol{f}_\Delta$ and $\boldsymbol{\tau}_\Delta$ from the flapping dynamics simplification can be deemed as the unmodeled dynamics. Moveover, $\boldsymbol{f}_\Delta$ and $\boldsymbol{\tau}_\Delta$ can include the error component from parameter uncertainties as well.*

The kinematics of the ship can be expressed as [40, 41]

$$\begin{cases} \dot{\boldsymbol{\xi}}_2 = \boldsymbol{R}_{t_2}\boldsymbol{V}_2 \\ \dot{\boldsymbol{\eta}}_2 = \boldsymbol{R}_{r_2}\boldsymbol{\Omega}_2 \end{cases} \tag{5}$$

where $\boldsymbol{\xi}_2 = [x_2, y_2, z_2]^T$ and $\boldsymbol{\eta}_2 = [\phi_2, \theta_2, \psi_2]^T$ are the position vector and attitude vector of the ship in the frame $\mathcal{F}_e$, respectively. $\boldsymbol{V}_2 = [u_2, v_2, w_2]^T$ and $\boldsymbol{\Omega}_2 = [p_2, q_2, r_2]^T$ are the velocity and the angular velocity of the ship defined in the frame $\mathcal{F}_c$, respectively. $\boldsymbol{R}_{t_2}$ and $\boldsymbol{R}_{r_2}$ are given by

$$\boldsymbol{R}_{t_2} = \begin{bmatrix} \mathrm{c}_{\theta_2}\mathrm{c}_{\psi_2} & \mathrm{s}_{\theta_2}\mathrm{c}_{\psi_2}\mathrm{s}_{\phi_2} - \mathrm{s}_{\psi_2}\mathrm{c}_{\phi_2} & \mathrm{s}_{\theta_2}\mathrm{c}_{\psi_2}\mathrm{c}_{\phi_2} + \mathrm{s}_{\psi_2}\mathrm{s}_{\phi_2} \\ \mathrm{c}_{\theta_2}\mathrm{s}_{\psi_2} & \mathrm{s}_{\theta_2}\mathrm{s}_{\psi_2}\mathrm{s}_{\phi_2} + \mathrm{c}_{\psi_2}\mathrm{c}_{\phi_2} & \mathrm{s}_{\theta_2}\mathrm{s}_{\psi_2}\mathrm{c}_{\phi_2} - \mathrm{c}_{\psi_2}\mathrm{s}_{\phi_2} \\ -\mathrm{s}_{\theta_2} & \mathrm{c}_{\theta_2}\mathrm{s}_{\phi_2} & \mathrm{c}_{\theta_2}\mathrm{c}_{\phi_2} \end{bmatrix}$$

$$\boldsymbol{R}_{r_2} = \frac{1}{\mathrm{c}_{\theta_2}} \begin{bmatrix} \mathrm{c}_{\theta_2} & \mathrm{s}_{\phi_2}\mathrm{s}_{\theta_2} & \mathrm{c}_{\phi_2}\mathrm{s}_{\theta_2} \\ 0 & \mathrm{c}_{\phi_2}\mathrm{c}_{\theta_2} & -\mathrm{s}_{\phi_2}\mathrm{c}_{\theta_2} \\ 0 & \mathrm{s}_{\phi_2} & \mathrm{c}_{\phi_2} \end{bmatrix}$$

The ship's motion involves the six degrees of freedom: pitch θ_2, heave z_2, roll ϕ_2, surge x_2, sway y_2, and yaw ψ_2. These motions are divided into two categories. The first three movements are induced by the sea waves, while the other movements are caused by the propellers and the sea waves. Thus, the dynamic equations of the ship can be expressed as [42, 43]

$$\begin{cases} \dot{u}_2 = \dfrac{m_{22}}{m_{11}}v_2 r_2 - \dfrac{d_{11}}{m_{11}}u_2 + \dfrac{1}{m_{11}}T_x + \dfrac{1}{m_{11}}d_{t_1} \\ \dot{v}_2 = -\dfrac{m_{11}}{m_{22}}u_2 r_2 - \dfrac{d_{22}}{m_{22}}v_2 + \dfrac{1}{m_{22}}T_y + \dfrac{1}{m_{22}}d_{t_2} \\ \dot{w}_2 = \zeta_1 \sin(\vartheta_1 t + \varrho_1) + d_{t_3} \\ \dot{p}_2 = \zeta_2 \sin(\vartheta_2 t + \varrho_2) + d_{s_1} \\ \dot{q}_2 = \zeta_3 \sin(\vartheta_3 t + \varrho_3) + d_{s_2} \\ \dot{r}_2 = \dfrac{m_{11} - m_{22}}{m_{33}}u_2 v_2 - \dfrac{d_{33}}{m_{33}}r_2 + \dfrac{1}{m_{33}}T_z + \dfrac{1}{m_{33}}d_{s_3} \end{cases} \tag{6}$$

where m_{ii} are given by the ship's inertia and the added mass effects, d_{ii} are given by the hydrodynamic damping. m_{ii} and d_{ii} $(i = 1, 2, 3)$ are assumed to be constant. T_x, T_y and T_z are the control forces and moments produced by the propellers. ζ_i and ϑ_i $(i = 1, 2, 3)$ are the motion coefficients that are dependent on the sea conditions. ζ_i represent the amplitude of the sea wave, ϑ_i the frequency and ι_i the initial phase. To include the random effects on the movements, ϱ_i are selected randomly. $\boldsymbol{d}_t = [d_{t_1}, d_{t_2}, d_{t_3}]^T$ and $\boldsymbol{d}_s = [d_{s_1}, d_{s_2}, d_{s_3}]^T$ are unknown bounded external disturbances.

Remark 2. *To aviod the complexity in the ship dynamics model, we use a simple physical model that consists of sinusoidal functions [43] and 3-DOF physical model [44, 45] in this paper.*

Remark 3. *The pitch, heave and roll motions of the ship can be sufficiently approximated using the sea wave model [43]. This is a commonly used approximation to describe the ship's motion since precise details of the ship's motion are not the focus of the study.*

3.3. Relative Motion Model

According to the helicopter and ship models proposed in the above subsection, define the relative postion and relative attitude in $\mathcal{F}_e$ as $\boldsymbol{\xi} = \boldsymbol{\xi}_1 - \boldsymbol{\xi}_2 = [x, y, z]^T$, $\boldsymbol{\eta} = \boldsymbol{\eta}_1 - \boldsymbol{\eta}_2 = [\psi, \theta, \phi]^T$, respectively. The relative velocity

$\boldsymbol{V} = \boldsymbol{V}_1 - \boldsymbol{R}_{t_2}\boldsymbol{V}_2$ is defined in $\mathcal{F}_e$, and the relative angular velocity $\boldsymbol{\Omega} = \boldsymbol{\Omega}_1 - \boldsymbol{R}_{r_{12}}\boldsymbol{\Omega}_2$ is defined in $\mathcal{F}_q$, where $\boldsymbol{R}_{r_{12}} = \boldsymbol{R}_{r_1}^{-1}\boldsymbol{R}_{r_2}$. Then, the relative model can be presented as

$$\begin{cases} \dot{\boldsymbol{\xi}} = \boldsymbol{V} \\ \ddot{\boldsymbol{\xi}} = -g\boldsymbol{e}_3 + \dfrac{T_m}{m}\boldsymbol{R}_{t_1}\boldsymbol{e}_3 - \dot{\boldsymbol{R}}_{t_2}\boldsymbol{V}_2 - \boldsymbol{R}_{t_2}\dot{\boldsymbol{V}}_2 + \Delta\boldsymbol{f} \\ \dot{\boldsymbol{\eta}} = \boldsymbol{R}_{r_1}\boldsymbol{\Omega} \\ \boldsymbol{I}\dot{\boldsymbol{\Omega}} = -\boldsymbol{\Omega}_1 \times \boldsymbol{I}\boldsymbol{\Omega}_1 + \boldsymbol{\tau}_\gamma - \boldsymbol{I}(\dot{\boldsymbol{R}}_{r_{12}}\boldsymbol{\Omega}_2 + \boldsymbol{R}_{r_{12}}\dot{\boldsymbol{\Omega}}_2) + \Delta\boldsymbol{\tau} \end{cases} \tag{7}$$

Remark 4. *During operation, the ship's states $\boldsymbol{V}_2$, $\dot{\boldsymbol{V}}_2$, $\boldsymbol{\Omega}_2$ and $\dot{\boldsymbol{\Omega}}_2$ can be obtained from the helicopter's states and relative states via the transformation formulae $\boldsymbol{V}_2 = \boldsymbol{R}_{t_2}^{-1}(\boldsymbol{V}_1 - \boldsymbol{V})$, $\dot{\boldsymbol{V}}_2 = \dot{\boldsymbol{R}}_{t_2}^{-1}(\boldsymbol{V}_1 - \boldsymbol{V}) + \boldsymbol{R}_{t_2}^{-1}(\dot{\boldsymbol{V}}_1 - \dot{\boldsymbol{V}})$, $\boldsymbol{\Omega}_2 = \boldsymbol{R}_{r_{12}}^{-1}(\boldsymbol{\Omega}_1 - \boldsymbol{\Omega})$, $\dot{\boldsymbol{\Omega}}_2 = \dot{\boldsymbol{R}}_{r_{12}}^{-1}(\boldsymbol{\Omega}_1 - \boldsymbol{\Omega}) + \boldsymbol{R}_{r_{12}}^{-1}(\dot{\boldsymbol{\Omega}}_1 - \dot{\boldsymbol{\Omega}})$. The relative motion states can either be measured from their inertial positions using high-accuracy GPS modules and inertial sensors [46], or by calculating directly via visual target tracking [47].*

3.4. Control Objective

For the subsequent development of ship landing control laws, the following assumptions are made.

Assumption 1. *The helicopter and ship are both rigid bodies. All states of ship are bounded under the effect of inputs.*

Assumption 2. *During flights, the Euler angles of the helicopter are always bounded as $\phi_1 \in (-\frac{\pi}{2}, \frac{\pi}{2})$ and $\theta_1 \in (-\frac{\pi}{2}, \frac{\pi}{2})$.*

Assumption 3. *$\Delta\boldsymbol{f}$ and $\Delta\boldsymbol{\tau}$ are differentiable and bounded, with their corresponding derivatives satisfying $\|\Delta\dot{\boldsymbol{f}}\| \leq L_1$ and $\|\Delta\dot{\boldsymbol{\tau}}\| \leq L_2$, where L_1 and L_2 are known constants.*

Remark 5. *Assumption 3 is reasonable since the unmodeled dynamics and the parameter uncertainties in $\Delta\boldsymbol{f}$ and $\Delta\boldsymbol{\tau}$ are restricted by helicopter's physical properties and are usually neglected. Also, the external disturbances, which are also included in $\Delta\boldsymbol{f}$ and $\Delta\boldsymbol{\tau}$, are bounded in practice.*

The control objective is to design control inputs T_m and $\boldsymbol{\tau}_\gamma$ for (7) such that the helicopter can land on the ship's deck steadily in fixed-time. To deal with the inherent underactuated property of the relative system, controller design is divided into two parts: RPC design and RAC design. In the first part, the RPC is designed to allow the state $\boldsymbol{\xi}$ to converge to $[0, 0, z_d]^T$ in fixed-time, where z_d is a known constant. In the second part, the RAC is designed to allow the convergence of the states z and $\boldsymbol{\Omega}$ to zero in fixed-time.

4. Control Design

In this section, as illustrated in Fig.3, detailed fixed-time control (FTC) algorithm design procedures are presented based on fixed-time observer and nonsingular terminal sliding mode technique.

4.1. Design of RPC

The RPC is designed for the approach phase which aims to bring the helicopter from a distant location to hover above the ship. Hence, the relative position $\boldsymbol{\xi}$ is desired to converge to $\boldsymbol{\xi}_d = [0, 0, z_d]^T$ under the control of RPC.

By defining the relative position error as $\Delta\boldsymbol{\xi} = \boldsymbol{\xi} - \boldsymbol{\xi}_d$, the relative position dynamics can be represented as

$$\begin{aligned} \Delta\ddot{\boldsymbol{\xi}} =& -g\boldsymbol{e}_3 + \frac{T_m}{m_1}\boldsymbol{R}_{t_1}\boldsymbol{e}_3 - \dot{\boldsymbol{R}}_{t_2}\boldsymbol{V}_2 - \boldsymbol{R}_{t_2}\dot{\boldsymbol{V}}_2 \\ &+ \Delta\boldsymbol{f} - \ddot{\boldsymbol{\xi}}_d \\ =& \boldsymbol{F}_1 + \boldsymbol{\Pi}_1 + \boldsymbol{d}_1 \end{aligned} \tag{8}$$

where $\boldsymbol{F}_1 = -g\boldsymbol{e}_3 - \dot{\boldsymbol{R}}_{t_2}\boldsymbol{V}_2 - \boldsymbol{R}_{t_2}\dot{\boldsymbol{V}}_2$, $\boldsymbol{\Pi}_1 = \frac{T_m}{m}\boldsymbol{R}_{t_1}\boldsymbol{e}_3$, $\boldsymbol{d}_1 = \Delta\boldsymbol{f}$. Describing the attitude error of the helicopter as $\Delta\boldsymbol{\eta}_1 = \boldsymbol{\eta}_1 - \boldsymbol{\eta}_{1d}$, the attitude error dynamics of the helicopter can be expressed as

$$\begin{aligned} \Delta\ddot{\boldsymbol{\eta}}_1 =& \dot{\boldsymbol{R}}_{r_1}\boldsymbol{\Omega}_1 - \boldsymbol{R}_{r_1}\boldsymbol{S}(\boldsymbol{\Omega}_1)\boldsymbol{\Omega}_1 + \boldsymbol{R}_{r_1}\boldsymbol{I}^{-1}\boldsymbol{\tau}_\gamma \\ &+ \boldsymbol{R}_{r_1}\boldsymbol{I}^{-1}\Delta\boldsymbol{\tau} - \ddot{\boldsymbol{\eta}}_{1d} \\ =& \boldsymbol{F}_2 + \boldsymbol{\Pi}_2 + \boldsymbol{d}_2 \end{aligned} \tag{9}$$

where $\boldsymbol{F}_2 = \dot{\boldsymbol{R}}_{r_1}\boldsymbol{\Omega}_1 - \boldsymbol{R}_{r_1}\boldsymbol{S}(\boldsymbol{\Omega}_1)\boldsymbol{\Omega}_1 - \ddot{\hat{\boldsymbol{\eta}}}_{1d}$, $\boldsymbol{\Pi}_2 = \boldsymbol{R}_{r_1}\boldsymbol{I}^{-1}\boldsymbol{\tau}_\gamma$, $\boldsymbol{d}_2 = \boldsymbol{R}_{r_1}\boldsymbol{I}^{-1}\Delta\boldsymbol{\tau} - \ddot{\boldsymbol{\eta}}_{1d} + \ddot{\hat{\boldsymbol{\eta}}}_{1d}$. $\ddot{\hat{\boldsymbol{\eta}}}_{1d}$ is the estimation value of the second derivative of $\boldsymbol{\eta}_{1_d}$. $\boldsymbol{\eta}_{1d} = [\phi_{1d}, \theta_{1d}, \psi_{1d}]^T$, ϕ_{1d} and θ_{1d} are obtained from (20). Although the commanded attitude $\boldsymbol{\eta}_{1d}$ is known, the computation of its second derivative is extremely intricate. Therefore, a second-order command filter is adopted to obtain the derivative.

$$\begin{cases} \dot{\boldsymbol{X}}_1 = \boldsymbol{X}_2 \\ \dot{\boldsymbol{X}}_2 = -2\Lambda\omega_n\boldsymbol{X}_2 - \omega_n^2(\boldsymbol{X}_1 - \boldsymbol{\eta}_{1d}) \end{cases} \tag{10}$$

where Λ is the damping ratio and ω_n is the damping frequency. The output of command filter are $\dot{\hat{\boldsymbol{\eta}}}_{1d} \triangleq \boldsymbol{X}_2$, $\ddot{\hat{\boldsymbol{\eta}}}_{1d} \triangleq \dot{\boldsymbol{X}}_2$.

Remark 6. *Setting ω_n that is sufficiently large and an appropriate Λ can guarantee fast tracking to the commanded attitude derivative signal, that is, the error $\ddot{\hat{\boldsymbol{\eta}}}_{1d} - \ddot{\boldsymbol{\eta}}_{1d}$ is bounded. Thus, $\boldsymbol{d}_2$ is also bounded and satisfy $\|\dot{\boldsymbol{d}}_2\| \leq L_2^*$, where L_2^* is a known constant.*

Step 1: Fixed-time Observer

Theorem 1. *Consider the relative position error dynamics (8) and the attitude error dynamics of the helicopter (9) under Assumption 4 and remark 5. Define ς_1, ς_2, ς_3 and ς_4 as the states of the developed fixed-time observer. If the observers are constructed as (11) and (12) and the following conditions hold for observer gains: $\lambda_1 > \sqrt{2\lambda_3}$,*

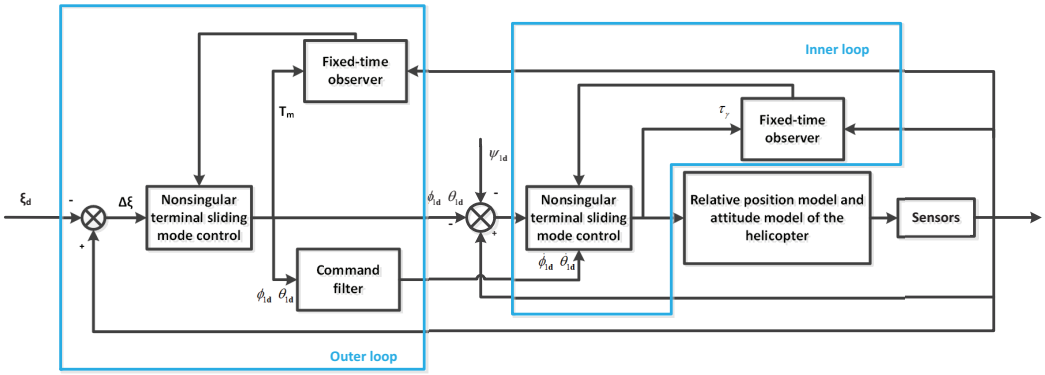

Figure 3: Schematic diagram of the fixed-time control algorithm

$\lambda_2 > 0$, $\lambda_3 > 4L_1$, $\lambda_4 > \sqrt{2\lambda_6}$, $\lambda_5 > 0$, $\lambda_6 > 4L_2^*$, *then the terms* $\boldsymbol{d}_1$ *and* $\boldsymbol{d}_2$ *can be estimated by* $\boldsymbol{\varsigma}_2$ *and* $\boldsymbol{\varsigma}_4$ *within fixed time, respectively.*

$$\begin{cases} \dot{\boldsymbol{\varsigma}}_1 = -\lambda_1 \dfrac{\boldsymbol{\kappa}_1}{\|\boldsymbol{\kappa}_1\|^{\frac{1}{2}}} - \lambda_2 \boldsymbol{\kappa}_1 \|\boldsymbol{\kappa}_1\|^{p_d - 1} + \boldsymbol{\varsigma}_2 + \boldsymbol{F}_1 + \boldsymbol{\Pi}_1 \\ \dot{\boldsymbol{\varsigma}}_2 = -\lambda_3 \dfrac{\boldsymbol{\kappa}_1}{\|\boldsymbol{\kappa}_1\|} \end{cases} \tag{11}$$

$$\begin{cases} \dot{\boldsymbol{\varsigma}}_3 = -\lambda_4 \dfrac{\boldsymbol{\kappa}_2}{\|\boldsymbol{\kappa}_2\|^{\frac{1}{2}}} - \lambda_5 \boldsymbol{\kappa}_2 \|\boldsymbol{\kappa}_2\|^{p_d - 1} + \boldsymbol{\varsigma}_4 + \boldsymbol{F}_2 + \boldsymbol{\Pi}_2 \\ \dot{\boldsymbol{\varsigma}}_4 = -\lambda_6 \dfrac{\boldsymbol{\kappa}_2}{\|\boldsymbol{\kappa}_2\|} \end{cases} \tag{12}$$

where $\boldsymbol{\kappa}_1 = \boldsymbol{\varsigma}_1 - \Delta\dot{\boldsymbol{\xi}}$, $\boldsymbol{\kappa}_2 = \boldsymbol{\varsigma}_3 - \Delta\dot{\boldsymbol{\eta}}_1$.

proof. By defining $\boldsymbol{\kappa}_3 = \boldsymbol{\varsigma}_2 - \boldsymbol{d}_1$, the error dynamics of the observer for $\boldsymbol{d}_1$ can be obtained as

$$\begin{cases} \dot{\boldsymbol{\kappa}}_1 = -\lambda_1 \dfrac{\boldsymbol{\kappa}_1}{\|\boldsymbol{\kappa}_1\|^{\frac{1}{2}}} - \lambda_2 \boldsymbol{\kappa}_1 \|\boldsymbol{\kappa}_1\|^{p_d - 1} + \boldsymbol{\kappa}_3 \\ \dot{\boldsymbol{\kappa}}_3 = -\lambda_3 \dfrac{\boldsymbol{\kappa}_1}{\|\boldsymbol{\kappa}_1\|} - \dot{\boldsymbol{d}}_1 \end{cases} \tag{13}$$

In accordance with the result in [48], when the observer gains satisfy the conditions in Theorem 1, both vector states $\boldsymbol{\kappa}_1$ and $\boldsymbol{\kappa}_3$ converge to the origin uniformly in fixed time:

$$T_0 \leq \left(\frac{1}{\lambda_2 (p_d - 1) \epsilon^{p_d - 1}} + \frac{2(\sqrt{2}\epsilon)^{\frac{1}{2}}}{\lambda_1} \right) \left(1 + \frac{\Gamma_1}{\Gamma_2 (1 - \sqrt{2\lambda_3}/\lambda_1)} \right) \tag{14}$$

where $\epsilon > 0$, $\Gamma_1 = \lambda_3 + L_1$, $\Gamma_2 = \lambda_3 - L_1$. The minimum value of $T_0(\epsilon)$ is achieved when $\epsilon = (2^{1/4}\lambda_1/\lambda_2)^{\frac{1}{p_d + \frac{1}{2}}}$. Therefore, the observer value $\boldsymbol{\varsigma}_2$ can approach $\boldsymbol{d}_1$ in fixed time T_0.

Similarly, it can be demonstrated that the observer value $\boldsymbol{\varsigma}_4$ can approach $\boldsymbol{d}_2$ in fixed time T_1.

$$T_1 \leq \left(\frac{1}{\lambda_5 (p_d - 1) \epsilon_1^{p_d - 1}} + \frac{2(\sqrt{2}\epsilon_1)^{\frac{1}{2}}}{\lambda_4} \right) \left(1 + \frac{\Gamma_3}{\Gamma_4 (1 - \sqrt{2\lambda_6}/\lambda_4)} \right) \tag{15}$$

where $\Gamma_3 = \lambda_6 + L_2^*$, $\Gamma_4 = \lambda_6 - L_2^*$, $\epsilon_1 > 0$, and the value of T_1 is minimum when $\epsilon_1 = (2^{1/4}\lambda_4/\lambda_5)^{\frac{1}{p_d + \frac{1}{2}}}$. The proof for the fixed-time observation of $\boldsymbol{d}_2$ is omitted here for the sake of space.

Step 2: Relative Postion Control

The terminal sliding surface is defined as

$$\boldsymbol{s}_1 = \Delta\boldsymbol{\xi} + (\boldsymbol{k}_1 \Delta\dot{\boldsymbol{\xi}})^{\lceil \frac{q_1}{p_1} \rfloor} \tag{16}$$

where $\boldsymbol{k}_1 = (\alpha_1 \langle \Delta\boldsymbol{\xi} \rangle^{m_1/n_1 - p_1/q_1} + \beta_1 \boldsymbol{E}_3)^{-1}$ and $\boldsymbol{E}_3$ is a three-dimensional unit matrix. m_1, n_1, p_1 and q_1 are positive odd integers satisfying the following: $m_1 > n_1$, $p_1 < q_1 < 2p_1$, $\alpha_1 > 0$ and $\beta_1 > 0$. Taking the first derivative of (16) yields

$$\begin{aligned} \dot{\boldsymbol{s}}_1 = & \Delta\dot{\boldsymbol{\xi}} + \frac{q_1}{p_1} \langle \boldsymbol{k}_1 \Delta\dot{\boldsymbol{\xi}} \rangle^{\frac{q_1}{p_1} - 1} (\boldsymbol{k}_1 (\boldsymbol{\Pi}_1 + \boldsymbol{F}_1 + \boldsymbol{d}_1) \\ & - \alpha_1 \left(\frac{m_1}{n_1} - \frac{p_1}{q_1} \right) \boldsymbol{k}_1^2 \langle \Delta\boldsymbol{\xi} \rangle^{\frac{m_1}{n_1} - \frac{p_1}{q_1} - 1} \Delta\dot{\boldsymbol{\xi}}^{\lceil 2 \rfloor} \Big) \end{aligned} \tag{17}$$

Therefore, a continuous fixed-time non-linear control law can be derived as

$$\begin{aligned} \boldsymbol{\Pi}_1 = & -\boldsymbol{F}_1 - \hat{\boldsymbol{d}}_1 + \boldsymbol{k}_1^{-1} \Bigg(\alpha_1 \boldsymbol{k}_1^2 \left(\frac{m_1}{n_1} - \frac{p_1}{q_1} \right) \\ & \times \langle \Delta\boldsymbol{\xi} \rangle^{\frac{m_1}{n_1} - \frac{p_1}{q_1} - 1} \Delta\dot{\boldsymbol{\xi}}^{\lceil 2 \rfloor} - \frac{p_1}{q_1} \boldsymbol{k}_1^{1 - \frac{q_1}{p_1}} \Delta\dot{\boldsymbol{\xi}}^{\lceil 2 - \frac{q_1}{p_1} \rfloor} \Bigg) \\ & - \frac{p_1}{q_1} \boldsymbol{k}_1^{-\frac{q_1}{p_1}} \boldsymbol{\mu}_t \langle \Delta\dot{\boldsymbol{\xi}} \rangle^{1 - \frac{q_1}{p_1}} \left(\alpha_2 \boldsymbol{s}_1^{\lceil \frac{m_2}{n_2} \rfloor} + \beta_2 \boldsymbol{s}_1^{\lceil \frac{p_2}{q_2} \rfloor} \right) \end{aligned} \tag{18}$$

where $\alpha_2 > 0$, $\beta_2 > 0$, and m_2, n_2, p_2, q_2 are positive odd integers satisfying $m_2 > n_2$ and $p_2 < q_2$. $\hat{\boldsymbol{d}}_1 = \boldsymbol{\varsigma}_2$ is the estimated value from the fixed-time observer. $\boldsymbol{\mu}_t = \mathrm{diag}\{\mu_t^1, \mu_t^2, \mu_t^3\}$, $\mu_t^i(\cdot)$ $(i = 1, 2, 3)$ is a function given by

$$\mu_t^i = \begin{cases} \sin \left(\dfrac{\pi}{2} \dfrac{\Delta\dot{\xi}_i^{q_1/p_1 - 1}}{\varpi_1} \right) & \Delta\dot{\xi}_i^{q_1/p_1 - 1} < \varpi_1 \\ 1 & \text{else} \end{cases} \tag{19}$$

where ϖ_1 is a small constant. Hence, the thrust control

input and desired attitude to the inner loop can be computed as

$$\begin{cases} \phi_{1d} = \arcsin\left(\frac{\Pi_{11}\sin\psi_{1d}-\Pi_{12}\cos\psi_{1d}}{\sqrt{\Pi_{11}^2+\Pi_{12}^2+\Pi_{13}^2}}\right) \\ \theta_{1d} = \arctan\left(\frac{\Pi_{11}\cos\psi_{1d}+\Pi_{12}\sin\psi_{1d}}{\Pi_{13}}\right) \\ T_m = m_1\sqrt{\Pi_{11}^2+\Pi_{12}^2+\Pi_{13}^2} \end{cases} \tag{20}$$

where Π_{11}, Π_{12} and Π_{13} are the first, second and third element of $\boldsymbol{\Pi}_1$.

Remark 7. *It should be metioned that a similar terminal sliding surface has been given in [49], expressed as*

$$\boldsymbol{s}^* = \boldsymbol{y}^* + a^*\langle|\boldsymbol{y}^*|\rangle^{a_1^*}sign(\boldsymbol{y}^*) + b^*\langle|\dot{\boldsymbol{y}}^*|\rangle^{a_2^*}sign(\dot{\boldsymbol{y}}^*) \tag{21}$$

where $a^*>0$, $b^*>0$, $1<a_2^*<2$, $a_1^*>a_2^*$. when $\boldsymbol{s}^*=\boldsymbol{0}$, we have $\dot{\boldsymbol{y}} = -b^{*-\frac{1}{a_2^*}}\langle|\boldsymbol{y}+a^*\langle|\boldsymbol{y}^*|\rangle^{a_1^*}sign(\boldsymbol{y}^*)|\rangle^{\frac{1}{a_2^*}}sign(\boldsymbol{y}+a^*\langle|\boldsymbol{y}^*|\rangle^{a_1^*}sign(\boldsymbol{y}^*))$, which can be verified that the fixed-tling time is bounded by $T^m < \left(\frac{b^*}{a^*}\right)^{\frac{1}{a_2^*}}\frac{1}{\frac{a_1^*}{a_2^*}-1} + b^{*\frac{1}{a_2^*}}\frac{1}{1-\frac{1}{a_2^*}}$. Compared with settling time in Lemma 1, $T^m > T$ for $b^*>1$ when $m/n = a_1^*/a_2^*$ and $p/q = 1/a_2^*$. Besides, a smaller $b^*<1$ in [49] results in a larger control input.

Step 3: Attitude Control

Define a terminal sliding manifold as

$$\boldsymbol{s}_2 = \Delta\boldsymbol{\eta}_1 + (\boldsymbol{k}_2\Delta\dot{\boldsymbol{\eta}}_1)^{\lceil\frac{q_3}{p_3}\rfloor} \tag{22}$$

where $\boldsymbol{k}_2 = (\alpha_3\langle\Delta\boldsymbol{\eta}_1\rangle^{m_3/n_3-p_3/q_3}+\beta_3\boldsymbol{E}_3)^{-1}$.

Similar with the control law of relative position control, the control input of the attitude control of the helicopter is designed as

$$\begin{aligned} \boldsymbol{\Pi}_2 = &-\boldsymbol{F}_2-\hat{\boldsymbol{d}}_2+\boldsymbol{k}_2^{-1}\left(\alpha_3\boldsymbol{k}_2^2\left(\frac{m_3}{n_3}-\frac{p_3}{q_3}\right)\right. \\ &\times\langle\Delta\boldsymbol{\eta}_1\rangle^{\frac{m_3}{n_3}-\frac{p_3}{q_3}-1}\Delta\dot{\boldsymbol{\eta}}_1^{[2]} - \frac{p_3}{q_3}\boldsymbol{k}_2^{1-\frac{q_3}{p_3}}\Delta\dot{\boldsymbol{\eta}}_1^{\left[2-\frac{q_3}{p_3}\right]}\Big) \\ &-\frac{p_3}{q_3}\boldsymbol{k}_2^{-\frac{q_3}{p_3}}\boldsymbol{\mu}_{t_2}\langle\Delta\dot{\boldsymbol{\eta}}_1\rangle^{1-\frac{q_3}{p_3}}\left(\alpha_4\boldsymbol{s}_2^{\lceil\frac{m_4}{n_4}\rfloor}+\beta_4\boldsymbol{s}_2^{\lceil\frac{p_4}{q_4}\rfloor}\right) \end{aligned} \tag{23}$$

where $\alpha_i>0$, $\beta_i>0$, and m_i, n_i, p_i, q_i are positive odd integers satisfying $m_i>n_i$, $(i=3,4)$, $p_3<q_3<2p_3$, $p_4<q_4$ and $m_3/n_3-p_3/q_3>1$. $\hat{\boldsymbol{d}}_2=\boldsymbol{\varsigma}_4$ is the estimation value of the fixed-time observer. $\boldsymbol{\mu}_{t_2}=\mathrm{diag}\{\mu_{t_2}^1,\mu_{t_2}^2,\mu_{t_2}^3\}$, $\mu_{t_2}^i(\cdot)$ $(i=1,2,3)$ is a function given by

$$\mu_{t_2}^i = \begin{cases} \sin\left(\frac{\pi}{2}\frac{\Delta\dot{\eta}_{1_i}^{q_3/p_3-1}}{\varpi_2}\right) & \Delta\dot{\eta}_{1_i}^{q_3/p_3-1} < \varpi_2 \\ 1 & \text{else} \end{cases} \tag{24}$$

where ϖ_2 is a small constant.

Theorem 2. *For the relative motion of the helicopter and ship system (7) under Assumptions 1-3, the proposed RPC described by (18) and (23) together with the fixed-time disturbance observer (11) and (12) can guarantee that the relative position error $\Delta\boldsymbol{\xi}$ and the attitude error of the helicopter $\Delta\boldsymbol{\eta}_1$ converge to zero in fixed-time, in which the settling time estimate can be estimated as*

$$T < T_{max} = T_d + T_t \tag{25}$$

where $T_t = max\{T_a,T_b\}+max\{T_e,T_f\}+\iota(\varpi_1,\varpi_2)$, ι is a small time margin bounded by $\iota_{max} = max\{2\varpi_1^{p_1/(q_1-p_1)}, 2\varpi_2^{p_3/(q_3-p_3)}\}$, $T_d = max\{T_0,T_1\}$.

$$\begin{aligned} T_a &= 6^{\frac{m_2-n_2}{2n_2}}\frac{1}{\alpha^*}\frac{n_2}{m_2-n_2}+\frac{1}{\beta^*}\frac{q_2}{q_2-p_2} \\ T_b &= 6^{\frac{m_4-n_4}{2n_4}}\frac{1}{\alpha^*}\frac{n_4}{m_4-n_4}+\frac{1}{\beta^*}\frac{q_4}{q_4-p_4} \\ T_e &= \frac{1}{\alpha_1}\frac{n_1}{m_1-n_1}+\frac{1}{\beta_1}\frac{q_1}{q_1-p_1} \\ T_f &= \frac{1}{\alpha_3}\frac{n_3}{m_3-n_3}+\frac{1}{\beta_3}\frac{q_3}{q_3-p_3} \end{aligned}$$

where $\alpha^*=min(\alpha_2,\alpha_4)$, $\beta^*=min(\beta_2,\beta_4)$.

proof. Consider the Lyapunov function candidate as

$$V_m = \frac{1}{2}\boldsymbol{s}_1^T\boldsymbol{s}_1+\frac{1}{2}\boldsymbol{s}_2^T\boldsymbol{s}_2 \tag{26}$$

With (18) and (23), the derivative of V_m is derived as

$$\begin{aligned} \dot{V}_m=&\boldsymbol{s}_1^T\dot{\boldsymbol{s}}_1+\boldsymbol{s}_2^T\dot{\boldsymbol{s}}_2 \\ =&-\boldsymbol{s}_1^T\boldsymbol{\mu}_t\left(\alpha_2\boldsymbol{s}_1^{\frac{m_2}{n_2}}+\beta_2\boldsymbol{s}_1^{\frac{p_2}{q_2}}\right)-\boldsymbol{s}_2^T\boldsymbol{\mu}_{t_2}\left(\alpha_4\boldsymbol{s}_2^{\frac{m_4}{n_4}}+\beta_4\boldsymbol{s}_2^{\frac{p_4}{q_4}}\right) \\ &+\frac{q_1}{p_1}\boldsymbol{s}_1^T\langle\boldsymbol{k}_1\Delta\dot{\boldsymbol{\xi}}\rangle^{\frac{q_1}{p_1}-1}\boldsymbol{k}_1(\boldsymbol{d}_1-\hat{\boldsymbol{d}}_1) \\ &+\frac{q_3}{p_3}\boldsymbol{s}_2^T\langle\boldsymbol{k}_2\Delta\dot{\boldsymbol{\eta}}_1\rangle^{\frac{q_3}{p_3}-1}\boldsymbol{k}_2(\boldsymbol{d}_2-\hat{\boldsymbol{d}}_2) \end{aligned} \tag{27}$$

By defining the estimate errors $\tilde{\boldsymbol{d}}_1=\boldsymbol{d}_1-\hat{\boldsymbol{d}}_1$ and $\tilde{\boldsymbol{d}}_2=\boldsymbol{d}_2-\hat{\boldsymbol{d}}_2$, Theorem 1 guarantees that the estimate errors converge to zero in fixed time, implying that $\tilde{\boldsymbol{d}}_1=\tilde{\boldsymbol{d}}_2=0$.

Then, equation (27) can be rewritten as

$$\begin{aligned} \dot{V}_m=&-\boldsymbol{s}_1^T\boldsymbol{\mu}_t\left(\alpha_2\boldsymbol{s}_1^{\frac{m_2}{n_2}}+\beta_2\boldsymbol{s}_1^{\frac{p_2}{q_2}}\right)-\boldsymbol{s}_2^T\boldsymbol{\mu}_{t_2}\left[\alpha_4\boldsymbol{s}_2^{\frac{m_4}{n_4}}+\beta_4\boldsymbol{s}_2^{\frac{p_4}{q_4}}\right] \\ \le&-\lambda_{\min}(\boldsymbol{\mu}_t)\alpha_2\left(\left(s_{11}^2\right)^{\frac{m_2+n_2}{2n_2}}+\left(s_{12}^2\right)^{\frac{m_2+n_2}{2n_2}}+\left(s_{13}^2\right)^{\frac{m_2+n_2}{2n_2}}\right) \\ &-\lambda_{\min}(\boldsymbol{\mu}_t)\beta_2\left(\left(s_{11}^2\right)^{\frac{p_2+q_2}{2q_2}}+\left(s_{12}^2\right)^{\frac{p_2+q_2}{2q_2}}+\left(s_{13}^2\right)^{\frac{p_2+q_2}{2q_2}}\right) \\ &-\lambda_{\min}(\boldsymbol{\mu}_{t_2})\alpha_4\left(\left(s_{21}^2\right)^{\frac{m_4+n_4}{2n_4}}+\left(s_{22}^2\right)^{\frac{m_4+n_4}{2n_4}}+\left(s_{23}^2\right)^{\frac{m_4+n_4}{2n_4}}\right) \\ &-\lambda_{\min}(\boldsymbol{\mu}_{t_2})\beta_4\left(\left(s_{21}^2\right)^{\frac{p_4+q_4}{2q_4}}+\left(s_{22}^2\right)^{\frac{p_4+q_4}{2q_4}}+\left(s_{23}^2\right)^{\frac{p_4+q_4}{2q_4}}\right) \\ \le&-\lambda_{\min}^*\alpha^*\left(\left(s_{11}^2\right)^{\frac{m^*+n^*}{2n^*}}+\left(s_{12}^2\right)^{\frac{m^*+n^*}{2n^*}}+\left(s_{13}^2\right)^{\frac{m^*+n^*}{2n^*}}\right. \\ &\left.+\left(s_{21}^2\right)^{\frac{m^*+n^*}{2n^*}}+\left(s_{22}^2\right)^{\frac{m^*+n^*}{2n^*}}+\left(s_{23}^2\right)^{\frac{m^*+n^*}{2n^*}}\right) \\ &-\lambda_{\min}^*\beta^*\left(\left(s_{11}^2\right)^{\frac{p^*+q^*}{2q^*}}+\left(s_{12}^2\right)^{\frac{p^*+q^*}{2q^*}}+\left(s_{13}^2\right)^{\frac{p^*+q^*}{2q^*}}\right. \\ &\left.+\left(s_{21}^2\right)^{\frac{p^*+q^*}{2q^*}}+\left(s_{22}^2\right)^{\frac{p^*+q^*}{2q^*}}+\left(s_{23}^2\right)^{\frac{p^*+q^*}{2q^*}}\right) \\ \le&-\lambda_{\min}^*\left(6^{\frac{n^*-m^*}{2n^*}}\alpha^*(2V_m)^{\frac{m^*+n^*}{2n^*}}+\beta^*(2V_m)^{\frac{p^*+q^*}{2q^*}}\right) \end{aligned} \tag{28}$$

where $\lambda^*_{\min} = \min(\lambda_{\min}(\boldsymbol{\mu}_t), \lambda_{\min}(\boldsymbol{\mu}_{t_2}))$, $\alpha^* = \min(\alpha_2, \alpha_4)$, $\beta^* = \min(\beta_2, \beta_4)$, and $m^* = m_2$, $n^* = n_2$, $p^* = p_2$, $q^* = q_2$ or $m^* = m_4$, $n^* = n_4$, $p^* = p_4$, $q^* = q_4$.

If $\dot{\xi}_i^{q_1/p_1-1} \geq \varpi_1$ and $\dot{\eta}_{1_i}^{q_3/p_3-1} \geq \varpi_2$, then $\mu_t^i = 1$ and $\mu_{t_2}^i = 1$. Thus, we have $\dot{V}_m \leq -6^{\frac{n^*-m^*}{2n^*}}\alpha_2(2V_m)^{\frac{m^*+n^*}{2n^*}} - \beta_2(2V_m)^{\frac{p^*+q^*}{2q^*}}$. Note that $V_m = 0$ implies $\boldsymbol{s}_1 = \boldsymbol{0}$ and $\boldsymbol{s}_2 = \boldsymbol{0}$. It follows from Lemma 1 and comparison principle that the sliding surfaces can be reached within the fixed time $t_m = max\{T_a, T_b\}$.

If $\dot{\xi}_i^{q_1/p_1-1} < \varpi_1$, $\dot{\eta}_{1_i}^{q_3/p_3-1} < \varpi_2$ and $\Delta\dot{\boldsymbol{\xi}} \neq 0$, $\Delta\dot{\boldsymbol{\eta}}_1 \neq 0$ then $0 < \mu_t^i < 1$, $0 < \mu_{t_2}^i < 1$. It can be similarly verified that the sliding surfaces are still reached within fixed time. If $\Delta\dot{\boldsymbol{\xi}} = 0$ and $\Delta\dot{\boldsymbol{\eta}}_1 = 0$, control inputs (18) and (23) are simplified as

$$\boldsymbol{\Pi}_1 = -\boldsymbol{F}_1 - \hat{\boldsymbol{d}}_1 - \frac{p_1}{q_1}\boldsymbol{k}_1^{-\frac{q_1}{p_1}}\left(\alpha_2\boldsymbol{s}_1^{\lceil m_2/n_2\rfloor} + \beta_2\boldsymbol{s}_1^{\lceil p_2/q_2\rfloor}\right)$$
$$\boldsymbol{\Pi}_2 = -\boldsymbol{F}_2 - \hat{\boldsymbol{d}}_2 - \frac{p_3}{q_3}\boldsymbol{k}_2^{-\frac{q_3}{p_3}}\left(\alpha_4\boldsymbol{s}_2^{\lceil m_4/n_4\rfloor} + \beta_4\boldsymbol{s}_2^{\lceil p_4/q_4\rfloor}\right)$$

Substituting the above control inputs into (8) and (9) yields

$$\Delta\ddot{\boldsymbol{\xi}} = -\frac{p_1}{q_1}\boldsymbol{k}_1^{-\frac{q_1}{p_1}}\left(\alpha_2\boldsymbol{s}_1^{\lceil m_2/n_2\rfloor} + \beta_2\boldsymbol{s}_1^{\lceil p_2/q_2\rfloor}\right)$$
$$\Delta\ddot{\boldsymbol{\eta}}_1 = -\frac{p_3}{q_3}\boldsymbol{k}_2^{-\frac{q_3}{p_3}}\left(\alpha_4\boldsymbol{s}_2^{\lceil m_4/n_4\rfloor} + \beta_4\boldsymbol{s}_2^{\lceil p_4/q_4\rfloor}\right)$$

Hence, we have $\Delta\ddot{\boldsymbol{\xi}} < 0$ for $s_{1i} > 0$, $\Delta\ddot{\boldsymbol{\xi}} > 0$ for $s_{1i} < 0$ and $\Delta\ddot{\boldsymbol{\eta}}_1 < 0$ for $s_{2i} > 0$, $\Delta\ddot{\boldsymbol{\eta}}_1 > 0$ for $s_{2i} < 0$. Then, we can conclude that the sliding surfaces $\boldsymbol{s}_1 = 0$ and $\boldsymbol{s}_2 = 0$ can be reached within a fixed time $T_t = max\{T_a, T_b\} + \iota(\varpi_1, \varpi_2)$, where $\iota(\varpi_1, \varpi_2)$ is determined by the boundary width $\iota_{max} = max\{2\varpi_1^{p_1/(q_1-p_1)}, 2\varpi_2^{p_3/(q_3-p_3)}\}$.

Once $\boldsymbol{s}_1 = 0$ and $\boldsymbol{s}_2 = 0$, this implies that

$$\Delta\dot{\boldsymbol{\xi}} = -\alpha_1\Delta\boldsymbol{\xi}^{\lceil\frac{m_1}{n_1}\rfloor} - \beta_1\Delta\boldsymbol{\xi}^{\lceil\frac{p_1}{q_1}\rfloor}$$
$$\Delta\dot{\boldsymbol{\eta}}_1 = -\alpha_3\Delta\boldsymbol{\eta}_1^{\lceil\frac{m_3}{n_3}\rfloor} - \beta_3\Delta\boldsymbol{\eta}_1^{\lceil\frac{p_3}{q_3}\rfloor}$$

Applying Lemma 1, it can be straightforwardly verified that the states $(\Delta\boldsymbol{\xi}, \Delta\dot{\boldsymbol{\xi}})$ and $(\Delta\boldsymbol{\eta}_1, \Delta\dot{\boldsymbol{\eta}}_1)$ will converge to the origin in fixed-time once the system trajectory reaches the sliding manifold and the boundaries of settling time is $t_n = max\{T_e, T_f\}$.

Therefore, the settling time is bounded by (25).

Remark 8. *In the proof, it should be indicated that the sliding surfaces $\boldsymbol{s}_1 = 0$ and $\boldsymbol{s}_2 = 0$ also can be reached under the condition $\dot{\xi}_i^{q_1/p_1-1} \geq \varpi_1$, $\dot{\eta}_{1_i}^{q_3/p_3-1} < \varpi_2$, or the condition $\dot{\xi}_i^{q_1/p_1-1} < \varpi_1$, $\dot{\eta}_{1_i}^{q_3/p_3-1} \geq \varpi_2$. This can be proved using the method described in the aforementioned section. The details are omitted herein for the sake of space.*

Remark 9. *By simplifying the fixed-time controller in (18) and (23), the finite-time controller can be expressed as* $\boldsymbol{\Pi}_1 = \frac{1}{\vartheta_t}\left(-\boldsymbol{F}_1 - \hat{\boldsymbol{d}}_1 - k_{\beta_1}\frac{p_1}{q_1}\Delta\boldsymbol{\xi}^{\lceil 2-\frac{p_1}{q_1}\rfloor} - k_{\alpha_1}\boldsymbol{s}_1^{\lceil\frac{m_1}{n_1}\rfloor}\right)$, $\boldsymbol{\Pi}_2 = \vartheta_\gamma^{-1}\left(-\boldsymbol{F}_2 - \hat{\boldsymbol{d}}_2 - k_{\beta_2}\frac{p_2}{q_2}\Delta\boldsymbol{\eta}_1^{\lceil 2-\frac{p_2}{q_2}\rfloor} - k_{\alpha_2}\boldsymbol{s}_2^{\lceil\frac{m_2}{n_2}\rfloor}\right)$, *with the sliding manifolds defined by* $\boldsymbol{s}_1 = \Delta\boldsymbol{\xi} + \frac{1}{k_{\alpha_1}}\Delta\dot{\boldsymbol{\xi}}$ *and* $\boldsymbol{s}_2 = \Delta\boldsymbol{\eta}_1 + \frac{1}{k_{\alpha_2}}\Delta\dot{\boldsymbol{\eta}}_1$, *where* $k_{\alpha_1}, k_{\alpha_2}$, k_{β_1}, k_{β_2} *are the control parameters. Furthermore, the traditional adaptive sliding mode method in [50] can be applied to autonomous ship landing as well. Comprehensive simulations based on the three control methods, that include the fixed-time method, finite-time method and traditional method, are carried out for the comparative analysis in the simulations section.*

Remark 10. *It's worth mentioning that the proposed control scheme can be applied even when the helicopter subjects to bounded time-varying actuator faults including multiplicative faults and additive faults. The additive faults can be incorporated in the lumped disturbances and estimated by the fixed-time disturbance observer, while the multiplicative faults can be compensated by adding a gain in the control input [51, 52].*

Remark 11. *Compared with the previous works [25, 26], the proposed terminal sliding mode control can overcome the singularity problem, which may result in the unboundness of the control input. Compared with the finite-time fault-tolerant contol method in [34], in which a fixed-time observer is also implemented, the proposed method can ensure that the tracking errors would converge to zero in fixed time in the presence of model uncertainties and external perturbations. Compared with the non-singular fixed-time control method in [37], which can also achieve fixed-time stability, the control signals of the proposed method are continuous without the use of a signum function. This enables the undesired chattering to be eliminated effectively.*

4.2. Design of RAC

As described above, the helicopter can be controlled to fly towards the ship and be in the hover position under the command of RPC. In this subsection, RAC is proposed to descend the helicopter vertically on the ship and synchronize the attitude of the helicopter and ship simultaneously. In view of the under-actuated property of the helicopter, we only consider the relative altitude and relative attitude of the helicopter and ship in RAC. Controlling the position in Oxy plane is beyond the scope of this paper. Therefore, it should be mentioned the landing phase will be fast so that the relative position of x and y can be as small as possible.

The relative altitude error and relative attitude error can be defined as $\Delta z = z - z_d$ and $\Delta\boldsymbol{\eta} = \boldsymbol{\eta} - \boldsymbol{\eta}_d$, respectively. To complete the descending phase, the desired value z_d and $\boldsymbol{\eta}_d$ are both specified as zero. Therefore, in order to simplify the relative position dynamics (8), the relative

altitude dynamics are expressed as

$$\begin{aligned}\Delta\ddot{z} &= -g + \frac{T_m}{m_1}\mathrm{c}_{\theta_1}\mathrm{c}_{\phi_1} - \dot{\boldsymbol{R}}_{t_2}^3\boldsymbol{V}_2 - \boldsymbol{R}_{t_2}^3\dot{\boldsymbol{V}}_2 + \Delta f_3 \\ &= F_3 + \Pi_3 + d_3\end{aligned} \tag{29}$$

where $F_3 = -g - \dot{\boldsymbol{R}}_{t_2}^3\boldsymbol{V}_2 - \boldsymbol{R}_{t_2}^3\dot{\boldsymbol{V}}_2$, $\Pi_3 = \frac{T_m^F}{m_1}\mathrm{c}_{\theta_1}\mathrm{c}_{\phi_1}$, $d_3 = \Delta f_3 + \frac{\phi_t}{m_1}\mathrm{c}_{\theta_1}\mathrm{c}_{\phi_1}$, where Δf_3 is the last element of $\Delta\boldsymbol{f}$. The relative attitude dynamics are represented as

$$\begin{aligned}\Delta\ddot{\boldsymbol{\eta}} =& \dot{\boldsymbol{R}}_{r_1}\boldsymbol{\Omega} - \boldsymbol{R}_{r_1}\boldsymbol{S}(\boldsymbol{\Omega}_1)\boldsymbol{\Omega}_1 + \boldsymbol{R}_{r_1}\boldsymbol{I}^{-1}\boldsymbol{\tau}_\gamma \\ &- \boldsymbol{R}_{r_1}(\dot{\boldsymbol{R}}_{\boldsymbol{r_{12}}}\boldsymbol{\Omega}_2 + \boldsymbol{R}_{r_{12}}\dot{\boldsymbol{\Omega}}_2) + \boldsymbol{R}_{r_1}\boldsymbol{I}^{-1}\boldsymbol{d}_2 \\ =& \boldsymbol{F}_4 + \boldsymbol{\Pi}_4 + \boldsymbol{d}_4\end{aligned} \tag{30}$$

where $\boldsymbol{F}_4 = \dot{\boldsymbol{R}}_{r_1}\boldsymbol{\Omega} - \boldsymbol{R}_{r_1}\boldsymbol{S}(\boldsymbol{\Omega}_1)\boldsymbol{\Omega}_1 - \boldsymbol{R}_{r_1}(\dot{\boldsymbol{R}}_{\boldsymbol{r_{12}}}\boldsymbol{\Omega}_2 + \boldsymbol{R}_{r_{12}}\dot{\boldsymbol{\Omega}}_2)$, $\boldsymbol{\Pi}_4 = \boldsymbol{R}_{r_1}\boldsymbol{I}^{-1}\boldsymbol{\tau}_\gamma^F$, $\boldsymbol{d}_4 = \boldsymbol{R}_{r_1}\boldsymbol{I}^{-1}(\Delta\boldsymbol{\tau} + \boldsymbol{\phi}_\gamma)$.

Remark 12. *Based on Assumption 4, d_3, $\boldsymbol{d}_4$ and their derivatives are all bounded, satisfying $|\dot{d}_3| \le L_3$ and $\|\dot{\boldsymbol{d}}_4\| \le L_4$.*

Theorem 3. *Consider the relative altitude error dynamics* (29) *and the relative attitude error dynamics* (30) *under remark 7. Define $\boldsymbol{\varsigma}_5$, $\boldsymbol{\varsigma}_6$, $\boldsymbol{\varsigma}_7$ and $\boldsymbol{\varsigma}_8$ as the states of the developed fixed-time observer. If the observers are constructed as* (31) *and* (32) *and the following conditions hold for observer gains: $\lambda_7 > \sqrt{2\lambda_9}$, $\lambda_8 > 0$, $\lambda_9 > 4L_3$, $\lambda_{10} > \sqrt{2\lambda_{12}}$, $\lambda_{11} > 0$, $\lambda_{12} > 4L_4$, then the terms d_3 and $\boldsymbol{d}_4$ can be estimated by $\boldsymbol{\varsigma}_6$ and $\boldsymbol{\varsigma}_8$ within fixed time T_2 and T_3, respectively.*

$$\begin{cases}\dot{\varsigma}_5 = -\lambda_7\dfrac{\kappa_3}{\|\boldsymbol{\kappa}_3\|^{\frac{1}{2}}} - \lambda_8\kappa_1|\kappa_1|^{p_d-1} + \varsigma_6 + F_3 + \vartheta_t\Pi_3 \\ \dot{\varsigma}_6 = -\lambda_9\dfrac{\kappa_3}{|\kappa_3|}\end{cases} \tag{31}$$

$$\begin{cases}\dot{\boldsymbol{\varsigma}}_7 = -\lambda_{10}\dfrac{\boldsymbol{\kappa}_4}{\|\boldsymbol{\kappa}_4\|^{\frac{1}{2}}} - \lambda_{11}\boldsymbol{\kappa}_4\|\boldsymbol{\kappa}_4\|^{p_d-1} + \boldsymbol{\varsigma}_8 + \boldsymbol{F}_4 + \boldsymbol{\vartheta}_\gamma\boldsymbol{\Pi}_4 \\ \dot{\boldsymbol{\varsigma}}_8 = -\lambda_{12}\dfrac{\boldsymbol{\kappa}_4}{\|\boldsymbol{\kappa}_4\|}\end{cases} \tag{32}$$

where $\kappa_3 = \varsigma_5 - \Delta\dot{z}$, $\boldsymbol{\kappa}_4 = \boldsymbol{\varsigma}_7 - \Delta\dot{\boldsymbol{\eta}}$.

$$T_2 \le \left(\frac{1}{\lambda_8(p_d-1)\epsilon_2^{p_d-1}} + \frac{2(\sqrt{2}\epsilon_2)^{\frac{1}{2}}}{\lambda_7}\right)\left(1 + \frac{\Gamma_5}{\Gamma_6(1-\sqrt{2\lambda_9}/\lambda_7)}\right)$$

$$T_3 \le \left(\frac{1}{\lambda_{11}(p_d-1)\epsilon_3^{p_d-1}} + \frac{2(\sqrt{2}\epsilon_3^{\frac{1}{2}}}{\lambda_{10}}\right)\left(1 + \frac{\Gamma_7}{\Gamma_8(1-\sqrt{2\lambda_{12}}/\lambda_{10})}\right)$$

where $\epsilon_2 > 0$, $\epsilon_3 > 0$, $\Gamma_5 = \lambda_9 + L_3$, $\Gamma_6 = \lambda_9 - L_3$, $\Gamma_7 = \lambda_{12} + L_4$, $\Gamma_8 = \lambda_{12} - L_4$.

proof. The proof is the same as Theorem 1.

Define terminal sliding manifolds as

$$s_3 = \Delta z + (k_3\Delta\dot{z})^{\frac{q_5}{p_5}} \tag{33}$$

$$\boldsymbol{s}_4 = \Delta\boldsymbol{\eta} + (\boldsymbol{k}_4\Delta\dot{\boldsymbol{\eta}})^{\lceil\frac{q_7}{p_7}\rfloor} \tag{34}$$

where $k_3 = 1/(\alpha_5\Delta z^{m_5/n_5 - p_5/q_5} + \beta_5)$, $\boldsymbol{k}_4 = (\alpha_7\langle\Delta\boldsymbol{\eta}\rangle^{m_7/n_7 - p_7/q_7} + \beta_7\boldsymbol{E}_3)^{-1}$.

Hence, the control law of relative altitude control and relative attitude control are designed respectively as

$$\begin{aligned}\Pi_3 =& -F_3 - \hat{d}_3 + k_3^{-1}\left(\alpha_5 k_3^2\left(\frac{m_5}{n_5} - \frac{p_5}{q_5}\right)\right. \\ &\times\Delta z^{\frac{m_5}{n_5}-\frac{p_5}{q_5}-1}\Delta\dot{z}^2 - \frac{p_5}{q_5}k_3^{1-\frac{q_5}{p_5}}\Delta\dot{z}^{2-\frac{q_5}{p_5}}\Big) \\ &- \frac{p_5}{q_5}k_3^{-\frac{q_5}{p_5}}\mu_{t_3}\Delta\dot{z}^{1-\frac{q_5}{p_5}}\left(\alpha_6 s_3^{\frac{m_6}{n_6}} + \beta_6 s_3^{\frac{p_6}{q_6}}\right)\end{aligned} \tag{35}$$

$$\begin{aligned}\boldsymbol{\Pi}_4 =& -\boldsymbol{F}_4 - \hat{\boldsymbol{d}}_4 + \boldsymbol{k}_4^{-1}\left(\alpha_7\boldsymbol{k}_4^2\left(\frac{m_7}{n_7} - \frac{p_7}{q_7}\right)\right. \\ &\times\langle\Delta\boldsymbol{\eta}\rangle^{\frac{m_7}{n_7}-\frac{p_7}{q_7}-1}\Delta\dot{\boldsymbol{\eta}}^{[2]} - \frac{p_7}{q_7}\boldsymbol{k}_4^{1-\frac{q_7}{p_7}}\Delta\dot{\boldsymbol{\eta}}^{[2-\frac{q_7}{p_7}]}\Big) \\ &- \frac{p_7}{q_7}\boldsymbol{k}_4^{-\frac{q_7}{p_7}}\boldsymbol{\mu}_{t_4}\langle\Delta\dot{\boldsymbol{\eta}}\rangle^{1-\frac{q_7}{p_7}}\left(\alpha_8\boldsymbol{s}_4^{\lceil\frac{m_8}{n_8}\rfloor} + \beta_8\boldsymbol{s}_4^{\lceil\frac{p_8}{q_8}\rfloor}\right)\end{aligned} \tag{36}$$

where $\alpha_i > 0$, $\beta_i > 0$, m_i, n_i, p_i, q_i are positive odd integers satisfying $m_i > n_i$, $(i = 5, 6, 7, 8)$, $p_k < q_k < 2p_k$, $m_k/n_k - p_k/q_k > 1$, $(k = 5, 7)$ and $p_l < q_l$, $(l = 6, 8)$. μ_{t_3} and $\boldsymbol{\mu}_{t_4} = \mathrm{diag}\{\mu_{t_4}^1, \mu_{t_4}^2, \mu_{t_4}^3\}$ $(i = 1, 2, 3)$ are given by

$$\mu_{t_3} = \begin{cases}\sin\left(\dfrac{\pi}{2}\dfrac{\Delta\dot{z}^{q_5/p_5-1}}{\varpi_3}\right) & \Delta\dot{z}^{q_5/p_5-1} < \varpi_3 \\ 1 & \text{else}\end{cases} \tag{37}$$

$$\mu_{t_4}^i = \begin{cases}\sin\left(\dfrac{\pi}{2}\dfrac{\Delta\dot{\eta}_i^{q_7/p_7-1}}{\varpi_4}\right) & \Delta\dot{\eta}_i^{q_7/p_7-1} < \varpi_4 \\ 1 & \text{else}\end{cases} \tag{38}$$

Theorem 4. *For the relative motion of the helicopter and ship system* (7) *under Assumptions 1-3, the proposed RAC described by* (35) *and* (36) *together with the fixed-time disturbance observer* (31) *and* (32) *can guarantee that the relative altitude error Δz and the relative attitude error $\Delta\boldsymbol{\eta}$ converge to zero in fixed-time. The corresponding settling time estimate is determined as follows*

$$T^* < T_{max}^* = T_d^* + T_t^* \tag{39}$$

where $T_t^* = max\{T_a^*, T_b^*\} + max\{T_e^*, T_f^*\} + \iota^*(\varpi_3, \varpi_4)$, ι^* is a small time margin bounded by $\iota_{max}^* = max\{2\varpi_3^{p_5/(q_5-p_5)}, 2\varpi_4^{p_7/(q_7-p_7)}\}$, $T_d^* = max\{T_2, T_3\}$.

$$T_a^* = 6^{\frac{m_6-n_6}{2n_6}}\frac{1}{\bar{\alpha}}\frac{n_6}{m_6-n_6} + \frac{1}{\bar{\beta}}\frac{q_6}{q_6-p_6}$$

$$T_b^* = 6^{\frac{m_8-n_8}{2n_8}}\frac{1}{\bar{\alpha}}\frac{n_8}{m_8-n_8} + \frac{1}{\bar{\beta}}\frac{q_8}{q_8-p_8}$$

$$T_e^* = \frac{1}{\alpha_5}\frac{n_5}{m_5-n_5} + \frac{1}{\beta_5}\frac{q_5}{q_5-p_5}$$

$$T_f^* = \frac{1}{\alpha_7}\frac{n_7}{m_7-n_7} + \frac{1}{\beta_7}\frac{q_7}{q_3-p_7}$$

where $\bar{\alpha} = min(\alpha_6, \alpha_8)$, $\bar{\beta} = min(\beta_6, \beta_8)$.

proof. The proof is the same as Theorem 2.

5. Simulations

To verify the effectiveness of the proposed RPC and RAC, a sequence of numerical simulations have been conducted in this section. The model parameters of helicopter and ship are shown in Table (1) [53]. Some of the sample values of pitch, heave and roll motions coefficients ζ_i and ϱ_i in different sea state are listed in Table (2) [43].

Wind model is established based on the consideration of the three main components: steady wind, atmospheric turbulence and gusts. The equivalent turbulence can be obtained using a shaping filter with white noise input. The transfer function of the shaping filter are [43] $T_x(s) = \sigma_x\sqrt{q_x}\frac{1.258s+5.033q_x}{s^2+6.829q_x s+5.033q_x^2}, T_j(s) = \sigma_j\sqrt{q_j}\frac{2.208s^2+17.855q_j s+6.498q_j^2}{s^3+12.836q_j s^2+6.498q_j^3}$, where $j = y, z$, $\sigma_i (i = x, y, z)$ is the turbulence intensity, $q_i = \frac{V_{wind}}{L_i}$, where V_{wind} is vertical component of trimmed speed, L_i is the turbulence length scale. The model can be extended to rotational velocity components in the same form. Steady wind and gusts are depicted by the combination of constant and '1-cosine' model.

$$\begin{bmatrix} W_x \\ W_y \\ W_z \end{bmatrix} = \begin{bmatrix} W_\phi \\ W_\theta \\ W_\psi \end{bmatrix} = \begin{bmatrix} 0.5 - 0.04\cos(0.5t) \\ 0.5 + 0.05\cos(0.5t) \\ 0.5 - 0.03\cos(0.5t) \end{bmatrix}.$$

5.1. Simulations of RPC

The simulation of RPC is performed based on the conditions in sea state 2. The desired relative position and desired yaw of the helicopter are set as $\boldsymbol{\xi}_d = [0, 0, 0.5]$m and $\psi_{1d} = \pi/8$, respectively. The initial conditions of the helicopter and ship are selected as $\boldsymbol{\xi}_1(0) = [6, 6, 5]^T$m, $\boldsymbol{V}_1(0) = [0.1, 0.1, 0.1]^T$m/s, $\boldsymbol{\eta}_1(0) = [0.1, 0.1, 0.1]^T$rad, $\boldsymbol{\Omega}_1(0) = [0.1, 0.1, 0.1]^T$rad/s, $\boldsymbol{\xi}_2(0) = [1, 1, 0]^T$m, $\boldsymbol{\eta}_2(0) = [0, 0, 0]^T$rad, $\boldsymbol{V}_2(0) = [0, 0, 0]^T$m/s, $\boldsymbol{\Omega}_2(0) = [0, 0, 0]^T$rad/s. The terminal sliding mode control parameters are chosen as $\alpha_1 = 0.02, \beta_1 = 0.5, \alpha_2 = \beta_2 = 1.3, m_1 = m_3 = 9, n_1 = n_3 = 5, p_1 = p_3 = 7, q_1 = q_3 = 9, m_2 = m_4 = 5, n_2 = n_4 = 3, p_2 = p_4 = 5, q_2 = q_4 = 9, \varepsilon_1 = \varepsilon_2 = 0.4, \omega_n = 25, \Lambda = 1.5$. The fixed-time disturbance observer parameters are $p_d = 1.5, \lambda_1 = 3, \lambda_2 = 0.5, \lambda_3 = 4, \lambda_5 = 0.2, \lambda_6 = 0.5$. The wind disturbances' parameters are set as $\sigma_i = 2, (i = x, y, z, \phi, \theta, \psi), L_x = L_z = L_\phi = L_\psi = 23$m, $L_\theta = L_y = 3$m, $V_{wind} = 10$m/s.

Table 1: Model parameters for helicopter and ship

parameter	value	parameter	value
m	7.4kg	m_{11}	150kg
I_x	0.16kgm^2	m_{22}	150kg
I_y	0.3kgm^2	m_{33}	100kgm^2
I_z	0.31kgm^2	d_{11}	150kg/s
M_a	25.23	d_{22}	150kg/s
L_b	25.23	d_{33}	100kgm^2/s
l_m	0.01m	T_x	100N
h_m	0.14m	T_y	-50N
l_t	0.95m	T_z	0Nm
h_t	0.05m	C_t	0.005
C_m	0.004	D_t	0.008
D_m	0.63		

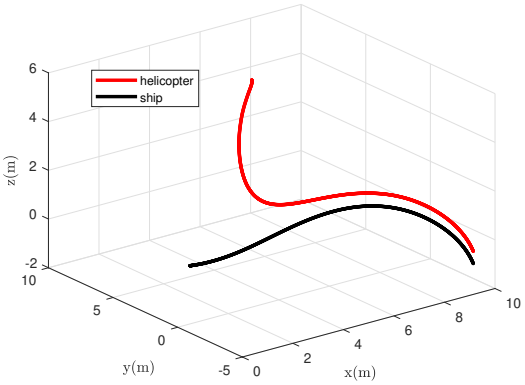

Figure 4: Trajectories of helicopter and ship in RPC

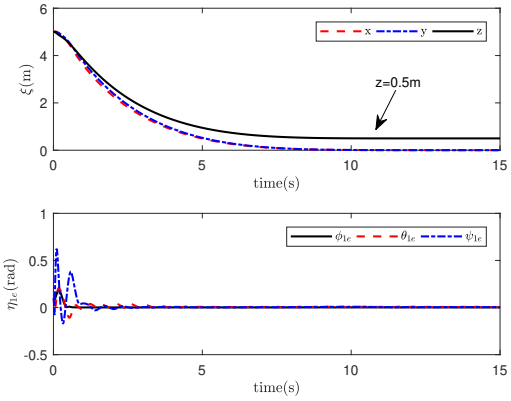

Figure 5: Relative position and attitude errors of helicopter in RPC

Table 2: Sample amplitudes and frequencies

sea state	2	6
pitch amplitude,deg	0.399	4.791
heave amplitude,m	0.137	1.652
roll amplitude,deg	0.216	2.59
pitch frequency,HZ	0.086	0.086
heave frequency,HZ	0.082	0.082
roll frequency,HZ	0.114	0.114

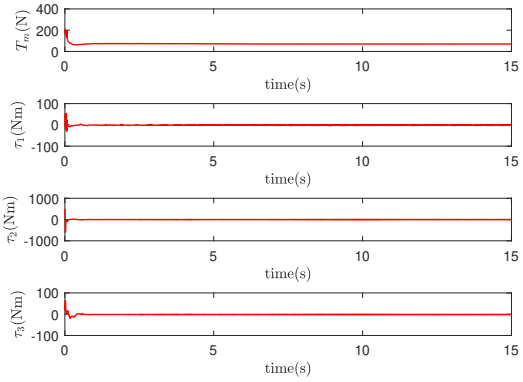

Figure 6: Control inputs of helicopter in RPC

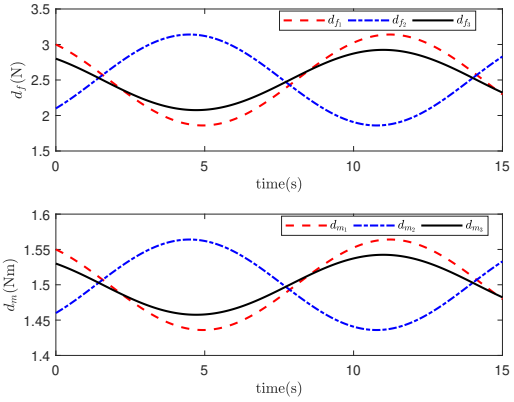

Figure 7: External disturbances in RPC

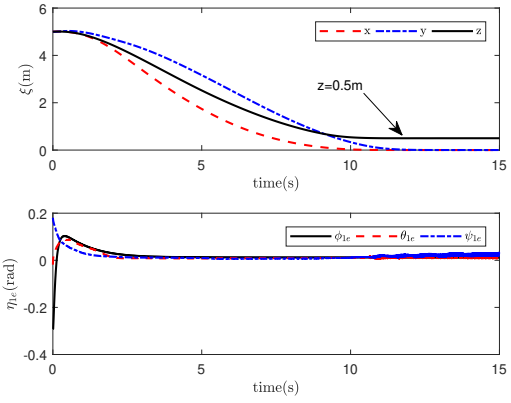

Figure 8: Relative position and attitude errors of helicopter in finite-time method

Figs.4-7 describe the simulation results of RPC. Fig.4 shows the motion trajectories of helicopter and ship in approach phase. It can be observed that the helicopter is able to track the ship's trajectory in the Oxy plane and maintains its flight at 0.5m above the ship under the control of RPC. Fig.5 demonstrates that the relative position

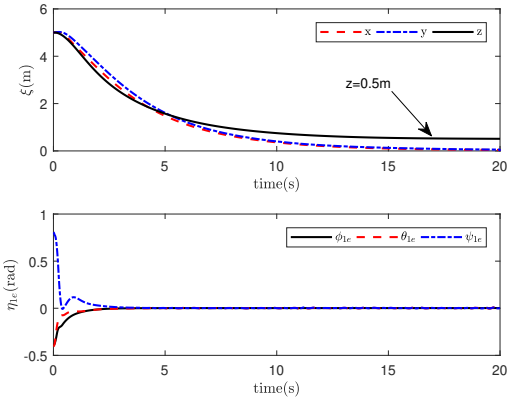

Figure 9: Relative position and attitude errors of helicopter in method [50]

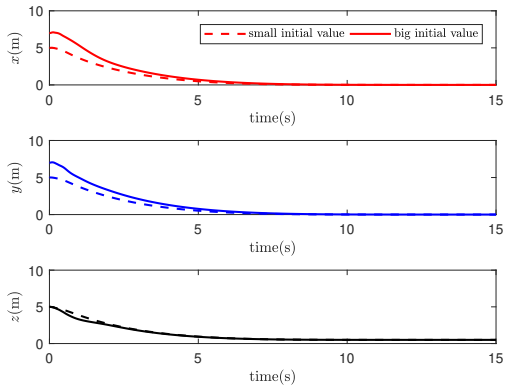

Figure 10: Comparisons between different initial conditions of proposed method

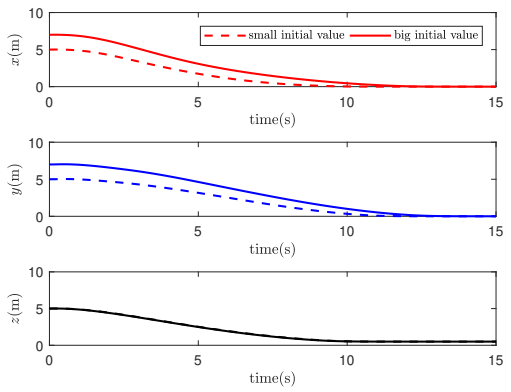

Figure 11: Comparisons between different initial conditions of finite-time method

in the Oxy plane and the relative altitude converge to zero and 0.5 respectively within 8s. This verifies that the estimated bound in Theorem 2 is reasonable. Meanwhile, the inner loop attitude errors of the helicopter converge to zero within 5s. The control input profiles are plotted in

Fig.6. Fig.7 describes the wind disturbances.

In order to highlight the advantages and effectiveness of the proposed fixed-time controller, the finite-time controller and the traditional controller in Remark 8 are utilized for the comparative analysis. The corresponding simulation results are depicted in Figs.8-9. It can be observed that the relative position converges to zero within 12s under the finite-time control, while the relative position converges to zero within 20s using the method in [50]. It is evident that the response time of finite-time method and method in [50] are both higher than the proposed fixed-time control method. Additionally, to show the comparative results more clearly and quantitatively, the performance comparisons of these methods are described in Table (3). IAE represents the integrated absolute error (defined as $\int_0^t |e(\tau)d\tau|$) and ITAE represents the integrated absolute error (defined as $\int_0^t t|e(\tau)d\tau|$). The IAE and ITAE metrics are introduced to evaluate the transient performance and the steady-state performance of the controller [54]. Furthermore, as shown in Fig.10-11, large initial values have no effect on the convergence time of the fixed-time control, while a longer convergence time is required when large initial values are used in the finite-time method. Therefore, it has been shown that the proposed control algorithm can achieve the control objective and provide a better performance as well.

5.2. Simulations of RAC

In accordance to the final conditions in RPC, the initial conditions of the helicopter and ship in RAC are specified as $\boldsymbol{\xi}_1(0) = [9.9, -3.45, -0.85]^T$m, $\boldsymbol{\eta}_1(0) = [0.39, 0.05, 0.02]^T$rad,$\boldsymbol{V}_1(0) = [0.46, -0.58, -0.3]^T$m/s, $\boldsymbol{\Omega}_1(0) = [0, 0, 0]^T$rad/s, $\boldsymbol{\xi}_2(0) = [9.9, -3.45, -1.35]^T$m, $\boldsymbol{\eta}_2(0) = [0.42, 0.67, 0.13]^T$rad, $\boldsymbol{V}_2(0) = [0.46, -0.58, -0.3]^T$m/s, $\boldsymbol{\Omega}_2(0) = [0, 0, 0]^T$rad/s. The fixed-time disturbance observer parameters are chosen the same as RPC. The control parameters are selected as $\alpha_5 = \beta_5 = 2.5, \alpha_6 = \beta_6 = 3, m_5 = m_7 = 9, n_5 = n_7 = 5, p_5 = p_7 = 7, q_5 = q_7 = 9, m_6 = m_8 = 5, n_6 = n_8 = 3, p_2 = p_4 = 5, q_6 = q_8 = 9, \varepsilon_3 = \varepsilon_4 = 0.1$.

As for wind disturbances, we established two typical simulations of wind conditions as shown Fig.12. Wind condition 1 (left figure in Fig.12) denotes that the steady wind disturbance is $0.5N$ and a turbulence intensity of $\sigma_i = 8(i = x, y, z, \phi, \theta, \psi)$, while wind condition 2 (right figure in Fig.12) represents a steady wind disturbance of $1N$ and turbulence intensity $\sigma_i = 15(i = x, y, z, \phi, \theta, \psi)$. The other wind parameters in these two conditions are the same as that used in RPC.

Table 3: Performance Comparisons of Different Methods

	error	fixed-time	finite-time	method in [50]
IAE	Δx	1172.1	2154.3	2609.8
	Δy	1216.8	3026.1	3259.4
	Δz	1071.9	2175	2646.4
ITAE	Δx	2.238×10^5	5.819×10^5	7.626×10^5
	Δy	2.359×10^5	2.082×10^6	3.494×10^6
	Δz	2.025×10^5	6.521×10^6	8.391×10^6

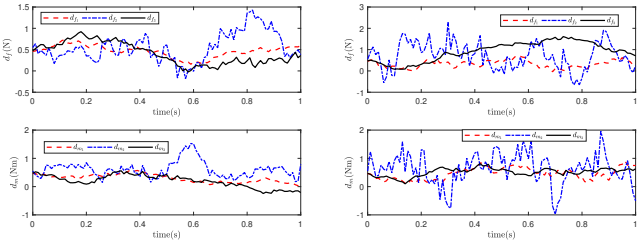

Figure 12: Wind disturbances in RAC

As demonstrated in Fig.13, the relative altitude and relative attitude of the helicopter and ship converge to zero within 1s. The corresponding the tracking errors in the Oxy plane are observed to $x = -0.21m$ and $y = -0.16m$ and hence satisfying the requirement of landing phase. Additionally, to verify the reliability of RAC, numerous simulations are repeated under different wind conditions and sea states. The results of the landing point in the Oxy plane are given in Fig.14, where the red cycle represents the landing point requirement boundary $R = 0.45m$, the green cycle is the available landing point boundary $R = 0.4m$ under the control of RAC at wind condition 1 and sea state 2. In the Fig.14, the blue cross-shaped points represent the landing points under wind condition 1 and sea state 2 (D1), black starlike points represent the landing points under wind condition 2 and sea state 2 (D2), pink square points represent the landing points under wind condition 1 and sea state 6 (D3). It¡¯s can be seen clearly that the tracking errors in Oxy plane remain within the required range under different intensity of disturbances, albeit a slight decrease in the control performance with higher intensity of the wind or wave disturbances.

Therefore, the proposed control strategy has been validated to be able to accomplish the task of landing the helicopter on a ship effectively.

6. Conclusions

The fixed-time autonomous shipboard landing of a helicopter with external disturbances is achieved in this paper. The process of shipboard landing is executed based on a fixed-time control scheme comprising of a nonsingular terminal sliding mode and a fixed-time disturbance observer. The utilization of fixed-time disturbance observer can estimate the lump disturbances and alleviate the undesired chattering in the control inputs effectively. Two controllers namely RPC and RAC, which are both designed in the framework of the fixed-time control algorithm, can ensure that the closed-loop systems errors converge to zero

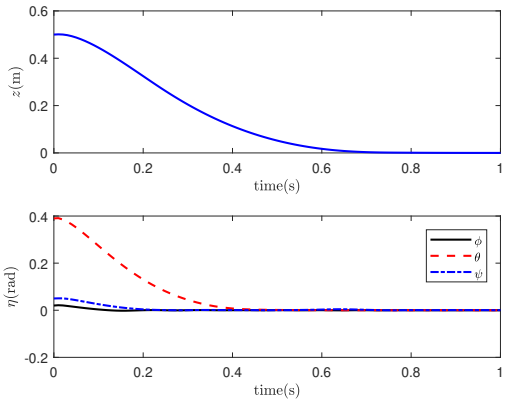

Figure 13: Relative altitude and relative attitude in RAC

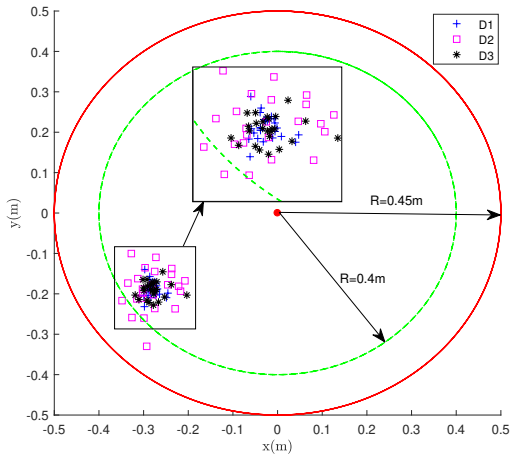

Figure 14: Landing points in RAC

in a fixed settling time. The results of multiple simulations verify that the proposed method can accomplish the autonomous shipboard landing operation in a fixed-time reliably. Particularly, comparative simulations results and quantitative analysis indicate that the proposed fixed-time method can provide a preferable and prompt control performance.

7. Acknowledgments

This work was supported by the National Natural Science Foundation of China (No.61503010), the Aeronautical Science Foundation of China (No.2016ZA51001), and the Fundamental Research Funds for the Central Universities (YWF-18-BJ-Y-108).

References

[1] Y. Zou, Adaptive trajectory tracking control approach for a model-scaled helicopter, Nonlinear Dynam. 83(4) (2016) 2171-2181.

[2] H. Shin, D. You, D. H. Shim, Autonomous shipboard landing algorithm for unmanned helicopters in crosswind, J. Intell. Robot. Syst. 74(1-2) (2014) 347-361.

[3] C. K. Tan, J. Wang, Y. C. Paw, F. Liao, Autonomous ship deck landing of a quadrotor using invariant ellipsoid method, IEEE Trans. Aero. Elec. Syst. 52(2) (2016) 891-903.

[4] A. A. Pashilkar, N. Sundararajan, P. Saratchandran, A fault-tolerant neural aided controller for aircraft auto-landing. Aerosp. Sci. Technol. 10(1) (2006) 49-61.

[5] S. Singh, R. Padhi, Automatic path planning and control design for autonomous landing of UAVs using dynamic inversion, American Control Conference (2009) 2409-2414.

[6] J. Ghommam, M. Saad, Autonomous landing of a quadrotor on a moving platform, IEEE Trans. Aerosp. Elec. Syst. 53(3) (2017) 1504-1519.

[7] J. Li, H. Duan, Simplified brain storm optimization approach to control parameter optimization in F/A-18 automatic carrier landing system, Aerosp. Sci. Technol. 42 (2015) 187-195.

[8] Z. Ma, T. Hu, L. Shen, Stereo vision guiding for the autonomous landing of fixed-wing UAVs: a saliency-inspired approach, Int. J. Adv. Robot. Syst. 13 (43) (2016) 1-13.

[9] S. Lin, M. A. Garratt, A. J. Lambert, Monocular vision-based real-time target recognition and tracking for autonomously landing an UAV in a cluttered shipboard environment, Auton. Robot. 41 (2017) 881-901.

[10] Y. Yan, D. Qi, C. Li, M. Yu, T. Chen, A Holistic Vision-based Hazard Detection Framework for Asteroid Landings, IFAC Paper Online, 49(17) (2016) 218-223.

[11] Y. Yu, H. Wang, N. Li, Z. Su, J. Wu, Automatic carrier landing system based on active disturbance rejection control with a novel parameters optimizer, Aerosp. Sci. Technol. 69 (2017) 149-160.

[12] Q. Lu, B. Ren, S. Parameswaran, Shipboard landing control enabled by an uncertainty and disturbance estimator, J. Guid. Control Dynam. 41(7) (2018) 1502-1520.

[13] Z. Peng, D. Wang, Z. Chen, X. Hu, W. Lan, Adaptive dynamic surface control for formations of autonomous surface vehicles with uncertain dynamics, IEEE Trans. Control Syst. Technol., 2013, 21(2):513-520.21(2) (2013) 513-520.

[14] J. L. Sanchez-Lopez, J. Pestana, S. Saripalli, P. Campoy, An approach toward visual autonomous ship board landing of a VTOL UAV. J. Intell. Robot. Syst. 74(1-2) (2014) 113-127.

[15] J. Zhang, S. Zhao, Y. Yang, Characteristic analysis for elliptical orbit hovering based on relative dynamics, IEEE Trans. Aero. Elec. Syst. 49(4) (2013) 2742-2750.

[16] X. Jin, Adaptive finite-time fault-tolerant tracking control for a class of MIMO nonlinear systems with output constraints, Int. J. Robust Nonlinear Control, 27 (2016) 722-741.

[17] X.Jin, Adaptive decentralized finite-time output tracking control for MIMO interconnected nonlinear systems with output constraints and actuator faults, Int. J. Robust Nonlinear Control, 28 (2018) 1808-1829.

[18] C. Li, Z. Qu, Distributed finite-time consensus of nonlinear systems under switching topologies, Automatica. 50(6) (2014) 1626-1631.

[19] Z. Zuo, Non-singular fixed-time terminal sliding mode control of non-linear systems, IET Control Theory A. 9(4) (2014) 545-552.

[20] A. Polyakov, Nonlinear feedback design for fixed-time stabilization of linear control systems, IEEE Trans. Autom. Control 57(8) (2012) 2106-2110.

[21] M. Zak, Terminal attractors for addressable memory in neural network, Phys. Lett. A 133(1-2) (1988) 18-22.

[22] Z. Man, X. Yu, Terminal sliding mode control of MIMO linear systems, IEEE Trans. Circuits Syst. I, Fundam. Theory Appl. 44(11) (1997) 823-830.

[23] Y. Zou, Nonlinear robust adaptive hierarchical sliding mode controlapproach for quadrotors, Int. J. Robust Nonlinear Control. 27 (2017) 925-941.

[24] M. Feroskhan, T. H. Go, Control strategy of sideslip perching maneuver under dynamic stall influence. Aerosp. Sci. Technol. 72 (2018) 150-163.

[25] M. Chen, Q. X. Wu, R. X. Cui, Terminal sliding mode track-

ing control for a class of SISO uncertain nonlinear systems, ISA Trans. 52(2) (2013) 198-206.
[26] Z. Zuo, L. Tie, A new class of finite-time nonlinear consensus protocols for multi-agent systems, Int. J. Control 87(2) (2014) 363-370.
[27] L. Yang, J. Yang, Nonsingular fast terminal sliding-mode control for nonlinear dynamical systems, Int. J. Robust. Nonlinear Control 21(16) (2011) 1865-1879.
[28] W. Chen, Disturbance observer based control for nonlinear systems, IEEE/ASME Trans. Mechatronics 9(4) (2004) 706-710.
[29] Z. Peng, J. Wang, D. Wang, Distributed containment maneuvering of multiple marine vessels via neurodynamics-based output feedback, IEEE Trans. Ind. Electron. 64(5) (2017) 3831-3839.
[30] Q. Hu, B. Li, J. Qi, Disturbance observer based finite-time attitude control for rigid spacecraft under input saturation, Aerosp. Sci. Technol. 39 (2014) 13-21.
[31] J. Yang, S. Li, J. Su, X. Yu, Continuous nonsingular terminal sliding mode control for systems with mismatched disturbances, Automatica 49(7) (2013) 2287-2291.
[32] Q. Lan, C. Qian, S. Li, Finite-time disturbance observer design and attitude tracking control of a rigid spacecraft, J. Dyn. Syst. Meas. Control 139(6) (2017) 061010 DOI:10.1115/1.4035457.
[33] M. Basin, P. Yu, Y. Shtessel, Hypersonic missile adaptive sliding mode control using finite- and fixed-Time Observers, IEEE Trans. Ind. Electron. 65(1) (2017) 930-941.
[34] X. Yu, P. Li, Y. Zhang, The design of fixed-time observer and finite-time fault-tolerant control for hypersonic gliding vehicles, IEEE Trans. Ind. Electron. 65(5) (2018) 4135-4144.
[35] S. R. Oh, K. Pathak, S. K. Agrawal, H. R. Pota, M. Garratt, Approaches for a tether-guided landing of an autonomous helicopter IEEE Trans. Robot. 22(3) (2006) 536-544.
[36] S. P. Bhat, D. S. Bernstein, Finite time stability of continuous autonomous systems, SIAM J. Control Optim. 38(3) (2009) 751-766.
[37] Z. Zuo, Non-singular fixed-time terminal sliding mode control of no-linear systems, IET Control Theory Appl. 9(4) (2015) 545-552.
[38] Y. Yang, C. Hua, J. Li, X. Guan, Robust adaptive uniform exact tracking control for uncertain euler¨Clagrange system, Int. J. Control 90(12) (2017) 2711-2720.
[39] Y. Zou, Z. Zheng, A robust adaptive RBFNN augmenting backstepping control approach for a model-scaled helicopter, IEEE Trans. Control Syst. Technol. 23(6) (2015) 2344-2352.
[40] T. Pérez, M. Blanke, Mathematical Ship Modeling for Control Applications, Technical Report (2002)
[41] Z. Peng, J. Wang, D. Wang, Senior Member, Containment Maneuvering of Marine Surface Vehicles With Multiple Parameterized Paths via Spatial-Temporal Decoupling, IEEE/ASME Trans. Mech. 22(2) (2017) 1026-1036.
[42] Z. Zheng, Y. Huang, L. Xie, B. Zhu, Adaptive trajectory tracking control of a fully actuated surface vessel with asymmetrically constrained input and output, IEEE Trans. Control Syst. Technol. (2017), https://doi.org/10.1109 /TCST.2017.2728518.
[43] S. Khantsis, Control system design using evolutionary algorithms for autonomous shipboard recovery of unmanned aerial vehicles, Ph.D. Thesis., Royal Melbourne Institute of Technology (2006).
[44] Z. Zheng, L. Sun, L. Xie, Error constrained LOS path following of a surface vessel with actuator saturation and faults, IEEE Trans. Syst., Man Cybernetics:Syst.(2017), https://doi.org/10.1109 /TSMC.2017.2717850.
[45] Z. Zheng, M. Feroskhan, Path following of a surface vessel with prescribed performance in the presence of input saturation and external disturbances, IEEE/ASME Trans. Mech. 22(6) (2017) 2564-2575.
[46] S. Oh, K. Pathak, S. Agrawal, H. Pota, M. Garratt, Approaches for a tether guided landing of an autonomous helicopter, IEEE Trans. Robotics. 22(3) (2006) 536-544.
[47] S. Saripalli, Vision-based autonomous landing of an helicopter on a moving target, AIAA Guidance, Navigation, and Control Conference, Chicago, Illinois, USA, August (2009) 10-13.
[48] M. Basin, C. B.Panathula, Y. Shtessel, Multivariable continuous fixed-time secondorder sliding mode control: design and convergence time estimation, IET Control Theory Appl. 11(8) (2017) 1104-1111.
[49] L. Yang, J. Yang, Nonsingular fast terminal sliding-mode control for nonlinear dynamical systems, Int. J. Robust. Nonlinear Control, 21(16) (2011) 1865-1879.
[50] K. Xia, W. Huo, Adaptive fault-tolerant control for cooperative spacecraft rendezvous and docking, American Control Conference (2017) 3747-3752.
[51] X. Jin, Fault tolerant finite-time leader-follower formation control for autonomous surface vessels with LOS range and angle constraints, Automatica. 68 (2016) 228-236.
[52] X. Jin, Fault-tolerant iterative learning control for mobile robots non-repetitive trajectory tracking with output constraints, Automatica. 94 (2018) 63-71.
[53] V. Gavrilets, Autonomous aerobatic maneuvering of miniature helicopter, Ph.D dissertation, Dept. Aeronaut. Astronaut., MIT, Cambridge, MA, USA, (2003).
[54] N. Wang, C. Qian, J. C. Sun, Y.C. Liu, Adaptive robust finite-time trajectory tracking control of fully actuated marine surface vehicles, IEEE Trans. Control Syst. Technol. 24(4) (2016) 1454-1462.